

Revealing Decurve Flows for Generalized Graph Propagation

Chen Lin ^{*1}, Liheng Ma ^{*2}, Yiyang Chen ^{*1}, Wanli Ouyang³,
Michael M. Bronstein¹, and Philip H.S. Torr¹

¹University of Oxford

²McGill University

³University of Sydney

February 14, 2024

Abstract

This study addresses the limitations of the traditional analysis of message-passing, central to graph learning, by defining *generalized propagation* with directed and weighted graphs. The significance manifest in two ways. **Firstly**, we propose *Generalized Propagation Neural Networks (GPNNs)*, a framework that unifies most propagation-based graph neural networks. By generating directed-weighted propagation graphs with adjacency function and connectivity function, GPNNs offer enhanced insights into attention mechanisms across various graph models. We delve into the trade-offs within the design space with empirical experiments and emphasize the crucial role of the adjacency function for model expressivity via theoretical analysis. **Secondly**, we propose the *Continuous Unified Ricci Curvature (CURC)*, an extension of celebrated *Ollivier-Ricci Curvature* for directed and weighted graphs. Theoretically, we demonstrate that CURC possesses continuity, scale invariance, and a lower bound connection with the Dirichlet isoperimetric constant validating bottleneck analysis for GPNNs. We include a preliminary exploration of learned propagation patterns in datasets, a first in the field. We observe an intriguing “*decurve flow*” - a curvature reduction during training for models with learnable propagation, revealing the evolution of propagation over time and a deeper connection to over-smoothing and bottleneck trade-off.

1 Introduction

Propagation of vertex features is central to various graph models, including message-passing models (MPNNs) and graph transformers (GTs).

*These authors contributed equally to this work.

MPNNs pass features by the graph structure of incoming data, inherently capturing characteristics of the underlying graph structure [Hamilton et al., 2017, Veličković et al., 2018, Monti et al., 2017]. Propagation of MPNNs is carefully inspected by analyzing its expressivity and geometric properties based on undirected and unweighted graphs. In detail, the expressive power of message-passing is bounded by the first-order Weisfeiler-Lehman test (1-WL) [Xu et al., 2019, Chen et al., 2019]. Furthermore, MPNNs suffer from over-squashing [Alon and Yahav, 2020] and over-smoothing [Chen et al., 2020, Oono and Suzuki, 2019] phenomena due to the undesirable geometric properties of the graph structures (eg. molecule, knowledge graph) like bottlenecks and complete graphs.

On the other hand, graph transformers determine the propagation of features with “attention” [Vaswani et al., 2017]. Pioneering methods directly apply self-attention on graphs, suffering a lack of structural information [Dwivedi and Bresson, 2021] and can be potentially improved by injecting additional positional/structural encodings [Kreuzer et al., 2021a, Rampásek et al., 2022, Chen et al., 2022, Ma et al., 2023]. Although GTs have shown superior performance on various benchmarks and diverse heuristics, a clear understanding of how they gain their power remains elusive [Cai et al., 2023]. Specifically, GTs are considered propagating messages with a undirected-unweighted complete graph [Shirzad et al., 2023a]. However, a random walk on complete graph would soon converges to stable distribution which implies severe over-smoothing [Giraldo et al., 2022], contradicting the empirical success of GTs.

In this study, we demonstrate that the limitation of existing analysis on message propagation largely stems from the traditional focus on defining propagation within the realm of undirected and unweighted graphs. Challenging conventional boundaries, we conceptualize the **generalize propagation** with directed and weighted graphs. The significance of this generalization manifest in two ways.

Firstly, we introduce *Generalized Propagation Networks (GPNNs)*, which unify GTs, MPNNs, and their variants by adopting directed, weighted propagation graphs. Central to GPNNs is the *adjacency function*, mapping adjacency matrices to vertex pair embeddings, and the *connectivity function*, converting these embeddings and vertex features into scalar values. This framework advances the analysis of propagation in graph models by its inherent ability to model “attention”, which is neglected with undirected and unweighted modeling. For completeness, we show that GPNNs’ expressiveness is determined by their adjacency function theoretically. Furthermore, we provide a taxonomy (see Appendix E.1) for the models that belongs to GPNN family and showcase the high-level design choice in literature. Through empirical evaluations within the design space, we show the impact of adjacency and connectivity function and pinpointing the most effective configurations as well as ineffective ones.

Secondly, we propose the *Continuous Unified Ricci Curvature (CURC)*, extending the celebrated *Ollivier-Ricci (OR) Curvature* to directed and weighted graphs [Ollivier, 2009]. CURC is defined by Wasserstein distance between mean transition probabilities centered at each vertex and an asymmetric distance for vertex pairs. During the derivation of CURC, we give a stronger version of

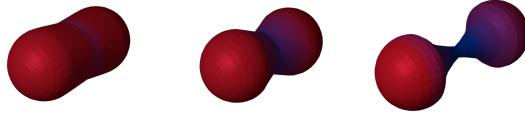


Figure 1: Geometric Flow Depicting Curvature Decrease.

This visual serves as an analogy for the curvature decrease observed in *Generalized Propagation Neural Networks (GPNNs)* with learnable propagation. The proposed *Continuous Uniform Ricci Curvature (CURC)* are applied to characterize this “*decurve flow*” observed across various models. Dark-blue and red represent regions of negative and positive curvature, respectively

Kantorovich-Rubinstein duality, which not only serves as the theoretical basis for our design of **reciprocal edge weight**, but also enables a wider class of valid distance function to create different graph curvatures based on Riemannian Geometry. Furthermore, three benign properties of CURC are demonstrated, which are particularly designed for generalized propagation graphs: (i) *continuity*, which enables smooth variation of the curvature with respect to the propagation graphs; (ii) unity with Ollivier-Ricci Curvature when the input graph is undirected and unweighted, when (u, v) and (v, u) coexist and both 1.0; and (iii) a lower bound linking CURC with the Dirichlet Isoperimetric Constant, validating the use of CURC in analyzing bottlenecks on graphs.

We analyze the geometric property of the generalized propagation for models with learnable propagation during training, which has been carried out for undirected-unweighted propagation with OR curvature by [Topping et al., 2022]. First in the field, we spotted the intriguing “*decurve flow*” phenomenon – a curvature reduction propagation graph evolution observed in multiple models, including the stat-of-the-art, during early stage in training. In contrast to rewiring [Topping et al., 2022], which increases curvature and reduces bottlenecks, generalized propagation graph of inspected models starts from a distribution of high curvatures and gradually decurves. This suggests a possible explanation of GTs performance: starting from an extreme curved state, GTs solves over-smoothing vs trade-off with respect to data.

2 Directed and Weighted Propagation

This section challenges the convention by defining message propagation on **directed-weighted** graphs. We show that directed-weighted propagation inherently provides insight to the “attention” mechanism in MPNNs. This analysis is extended towards a general graph model framework - GPNN, characterizing various propagation based methods. We finish this section with a discussion on its **design space** and an exhibition of GPNNs **expressivity**.

Preliminary In this work, we concern machine learning algorithms on undirected graphs $\mathcal{G} = (\mathcal{V}, \mathcal{E})$ characterized by two sets, namely the vertices $\mathcal{V} =$

$\{1, \dots, n\}$ and the edges $\mathcal{E} \subseteq \mathcal{V} \times \mathcal{V}$. Given the indexes of the vertices, the structure of the graph can also be represented by its adjacency matrix \mathbf{A} , where $a_{uv} = 1$ iff $(u, v) \in \mathcal{E}$ and zero otherwise. Each vertex and edge could be associated with attributes x_u and e_{uv} . The intermediate hidden variables passing between layers are denoted as h . A graph network model usually contains multiple layers marked as L .

Generalized Propagation We consider message propagation on weighted-directed graph $\mathcal{G}_p = (\mathcal{V}, \mathcal{E}, \omega)$, where ω denotes the connectivity: $\forall (u, v) \in \mathcal{E} \rightarrow \omega_{uv} \in \mathbb{R}$. The connectivity ω models the amount of information that is passed along with a specific edge (eg. ‘‘attention’’). In fact, the concept of weighted propagation is common and can be introduced to MPNNs by refining its definition (see Appendix C.1)

$$\begin{aligned} \omega_{vu}^{l+1} &= C_l(h_v^l, h_u^l, e_{vu}) \\ m_v^{l+1} &= \sum_{u \in N(v)} \omega_{vu}^l \cdot M_l(h_u^l) \end{aligned} \quad (1)$$

where C_l is a scalar function that models the connectivity. This formulation is standard in most MPNNs [Kipf and Welling, 2017, Monti et al., 2017, Veličković et al., 2018, Bresson and Laurent, 2018]. Previous analyses over message passing are based on the summation over neighbors, overlooking the important affect of connectivity.

GPNNs To obtain a general formulation, we make extentions: (1) summation over all vertices. (2) an **adjacency function** F , defined as a permutation equivariant mapping from the adjacency matrix \mathbf{A} and edge feature \mathbf{E} (if available) to its embedding f_{vu} . (3) the **connectivity function** which depend on adjacency feature f_{vu} and along with vertex features. The resulting formulation contains four steps for each layer,

$$\begin{aligned} f_{vu}^l &= [F_l(\mathbf{A}, \mathbf{E})]_{vu} \\ \omega_{vu}^{l+1} &= C_l(h_v^l, h_w^l, f_{vu}^l) \\ m_v^{l+1} &= \sum_{u \in \mathcal{V}} \omega_{vu}^{l+1} \cdot M_l(h_u^l) \\ h_v^{l+1} &= U_l(h_v^l, m_v^{l+1}) \end{aligned} \quad (2)$$

where $[\cdot]_{ij}$ indicates the (i, j) element of the input matrix/tensor.

2.1 GPNN Design Space

In Appendix E.2 we show existing methods belong to GPNNs by casting their formulation with GPNNs’ adjacency and connectivity function. GPNNs cover a wide range of propagation-based models, making them excellent guidelines for taxonomy (see Appendix E.1). Here we highlight several important design choices.

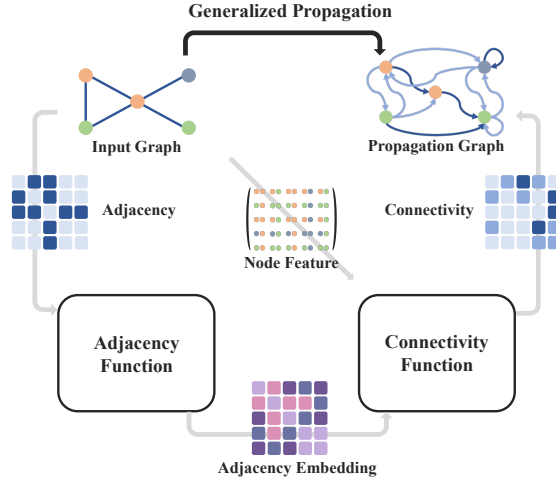


Figure 2: The demonstration of GPNN framework

Multi-head v.s. Single-head pinpointing the question of whether multiple propagation graphs should be used in each GPNN layer. When multi-head is adopted, ω_{uv}^l , m_v^l and h_v^l will be specific to each head as ω_{uv}^{lh} , m_v^{lh} and h_v^{lh} . The multi-head approach is adopted commonly with attention mechanisms.

Local v.s. Non-Local v.s. Global Propagation can be identified based on the constraints imposed by the input graph. Local propagation constrains the propagation graph to be a weighted version of the input graph, which is typical for MPNNs. Global propagation poses no constraint to the propagation graph, characterizing most GTs. Non-local propagation, making the propagation graph a super graph of the input graph, includes additional edges but does not form a complete graph to balance cost and expressiveness, incorporating techniques like graph-rewiring, polynomial spectral GNNs, diffusion-enhanced GNNs, and efficient GTs or MPNNs with virtual nodes.

Static v.s. Dynamic Propagation *static* mode denotes that all layers in GPNNs are sharing the same propagation graph. In contrast, the *dynamic* mode indicates that different propagation graphs are used in different layers. This is typically implemented by evolving the connectivity ω_{vu}^l across layers.

Feature-independent v.s. Feature-dependent Propagation The propagation graph can be generated in two ways: depending on the node features, referred to as *feature-dependent (Feat. Dep.)* propagation, commonly seen in models with attention or gating mechanisms. Otherwise, the propagation is referred to as *feature-independent (Feat. Ind.)* propagation. The adjacency function F_l , as the essential component in GPNNs, interprets the topological information contained in the adjacency matrix \mathbf{A} for the connectivity function. The adjacency functions can be as simple as performing normalization on adjacency matrix \mathbf{A} or the Laplacian matrix \mathbf{L} , as seen in many MPNNs. More complicated designs, such as computing power series of $\mathbf{A}(\mathbf{L})$ (polynomial

spectral/diffusion GNNs [Defferrard et al., 2016, Gasteiger et al., 2019, Frasca et al., 2020], GRIT [Ma et al., 2023]) or performing eigendecomposition on $\mathbf{A}(\mathbf{L})$ [Kreuzer et al., 2021a, Hussain et al., 2022], can explore richer topological information and facilitate connectivity function to generate more expressive propagation graphs.

2.2 Expressiveness of GPNNs

GPNNs subsume models with various expressiveness. However, by abstracting away the exact adjacency and mild assumption over connectivity function (MLPs), we deliver two propositions by inducting a common routine for propagation-based models expressivity assessment. To reach the upper-bounded expressiveness for both propositions, a sufficient number of heads, MLPs with a sufficient layer and width for the connectivity function, and an update function are required. First, we consider the GPNNs with static propagation for a sufficient number of heads and layers, referred to as *static GPNNs*.

Proposition 2.1. (*Static GPNNs*) *For a static GPNN model with a fixed adjacency feature $[f_{uv}]_{u,v \in \mathcal{V}}$ and sufficient heads and layers, the expressiveness is upper-bounded by the color refinement iteration*

$$\mathcal{X}_{\mathcal{G}}^{t+1}(v) = \text{hash}\{(\mathcal{X}_{\mathcal{G}}^t(u), f_{vu}) : u \in \mathcal{V}\} \quad (3)$$

The proof the proposition 2.1 is provided in Appendix B.2. This expressiveness result could be induced by existing expressivity proof in propagation-based GNNs. This proposition assured an expressiveness upper bound for models in GPNN families by solely inspecting their adjacency function.

Generally, we consider the unusual case when multiple adjacency function F_l is applied, rotating among layers, eg. [Rampášek et al., 2022].

Proposition 2.2. (*Dynamic GPNNs*) *Suppose a Layer-recurrent GPNN model M has a layer-dependent adjacency embedding repeats every p layer: $f_{vu}^l = f_{vu}^{l+p}, \forall v, u \in \mathcal{V}$. With sufficient heads and layers, by stacking of such repetition, the expressiveness of M is upper-bounded by the color refinement iteration*

$$\mathcal{X}_{\mathcal{G}}^{t+1}(v) = \text{hash}\{(\mathcal{X}_{\mathcal{G}}^t(u), (f_{vu}^1, f_{vu}^2, \dots, f_{vu}^p)) : u \in \mathcal{V}\} \quad (4)$$

We refer readers to Appendix B.2 for detailed proof. This proposition justified those approaches introducing multiple adjacency functions for different layers: the overall expressiveness is not weaker than the ones using any one of the adjacency functions alone. This proposition provides a strong theoretical foundation for the usage of *dynamic propagation* designs in GPNNs.

3 Continuous Unified Ricci Curvature

In the previous section, we generalize message propagation with directed-weighted graphs and carry out a general framework that characterizes various propagation-based graph models. In this section, we introduce the *Continuous Unified Ricci*

Curvature (CURC) designed explicitly for analyzing GPNNs’ weighted-directed propagation graph. Notably, we propose a stronger version of Kantorovich-Rubinstein duality, which serves as the theoretical basis for our design of reciprocal edge weight and enables a broader class of valid distance functions. Later, we discuss the connection between optimal transport and information propagation on graphs. Finally, we finish by analyzing the properties of CURC, including a lower bound connecting the Dirichlet isoperimetric constant and CURC.

3.1 Preliminaries for CURC

To facilitate comprehension of readers and maintain the notation consistency with earlier works on curvatures, we utilize function notation to describe CURC. For example, we interpret ω as a function $\omega : \mathcal{V} \times \mathcal{V} \mapsto \mathbb{R}^{\geq 0}$ where $\omega(v, u)$ is equivalent to ω_{vu} in Eq. 1. To avoid confusion with the notations in previous sections, we use x, y instead of v, u specifically in for CURC. Note that, for CURC, we only consider the absolute value of ω_{vu} . We assume all propagation graphs $\mathcal{G} = (\mathcal{V}, \mathcal{E}, \omega)$ in this section to be strongly-connected weighted-directed finite graphs with n vertices, except otherwise specified. Let the **random walk matrix** $W \in \mathbb{R}^{n \times n}$ be defined by $[W]_{xy} := d_x^{-1} \omega(x, y)$, where $d_x := \sum_{y \in \mathcal{V}} \omega(x, y)$. In the following discussions, we abuse the notation of W to keep in line with other function-form variables, where we denote $[W]_{xy}$ as $W(x, y)$. We construct CURC based on the curvature proposed by Ozawa et al. [2020] and Lin-Liu-Yau Ricci Curvature Lin et al. [2011].

3.2 Construction of CURC

According to the *Perron-Fronbenius Theorem* [Kirkwood and Kirkwood, 2020], for a finite strongly-connected weighted-directed graph $\mathcal{G} = (\mathcal{V}, \mathcal{E}, \omega)$, there exists a strictly positive left eigenvector $\mathbf{v}_{pf} \in \mathbb{R}^{1 \times n}$ of the corresponding random walk matrix W (*Perron-Frobenius left eigenvector*). By normalizing \mathbf{v}_{pf} , we state the following concept of **Perron measure**, which also corresponds to the stationary distribution for the random walk matrix W .

Definition 3.1. (Perron measure) For $\mathcal{G} = (\mathcal{V}, \mathcal{E}, \omega)$, let $\mathbf{v}_{pf} \in \mathbb{R}^{1 \times n}$ be its Perron-Frobenius left eigenvector. The *Perron measure* $\mathbf{m} : \mathcal{V} \mapsto (0, 1]$ is defined by

$$\mathbf{m}(x) := \left(\frac{\mathbf{v}_{pf}}{\|\mathbf{v}_{pf}\|} \right)_x.$$

Definition 3.2. (Mean transition probability kernel) Let $\mathbf{m} : \mathcal{V} \mapsto (0, 1]$ be the perron measure defined on graph $\mathcal{G} = (\mathcal{V}, \mathcal{E}, \omega)$. The *mean transition probability kernel* $\mu : \mathcal{V} \times \mathcal{V} \mapsto [0, 1]$ is defined by

$$\mu(x, y) := \begin{cases} \frac{1}{2} [W(x, y) + \frac{\mathbf{m}(y)}{\mathbf{m}(x)} W(y, x)] & \text{if } y \neq x \\ 0 & \text{if } y = x \end{cases} \quad (5)$$

where $\mu_x(y) := \mu(x, y)$ and $\sum_{y \in \mathcal{V}} \mu_x(y) = 1$ for fixed $x \in \mathcal{V}$.

Here, we can easily induce that $\sum_{y \in \mathcal{V}} \frac{m(y)}{m(x)} W(y, x) = 1$ by checking $\sum_{y \in \mathcal{V}} W(x, y) = 1$ and $\sum_{y \in \mathcal{V}} \frac{m(y)}{m(x)} W(y, x) = 1$. Intuitively, $\sum_y \frac{m(y)}{m(x)} W(y, x)$ contains the information of random walks from y to x . We aim to define curvature for weighted-directed graphs with Wasserstein distance by optimal transpor. We will use this mean transition probability kernel to construct initial mass distribution for the optimal transport [Ozawa et al., 2020]. In order to reduce the optimal transport problem to linear programming, K-R duality is essential. Conventionally, we require a distance function to be non-negative, definite, symmetric and satisfies the triangle inequality. In the following, we propose a version of K-R duality that requires a weaker condition on the distance function of graph \mathcal{G} , excluding the symmetry restriction.

Definition 3.3. (Coupling) Suppose μ and ν to be two probability distribution on finite sets \mathcal{X} and \mathcal{Y} respectively. Let $\Pi(\mu, \nu)$ denotes the set of *couplings* between μ and ν . We say $\pi : \mathcal{X} \times \mathcal{Y} \mapsto [0, 1] \in \Pi(\mu, \nu)$ is a *coupling* if

$$\sum_{y \in \mathcal{V}} \pi(x, y) = \mu(x), \quad \sum_{x \in \mathcal{V}} \pi(x, y) = \nu(y).$$

Theorem 3.4. (K-R duality) Let $\mathcal{G} = (\mathcal{V}, \mathcal{E}, \omega)$ be a graph with (asymmetric) distance function $d : \mathcal{V} \times \mathcal{V} \mapsto \mathbb{R}^{\geq 0}$ satisfying triangle inequality and admits $d(x, y) = 0$ if and only if $x = y$. Then for probability measure $\mu, \nu : \mathcal{V} \mapsto [0, 1]$, the **Kantorovich-Rubinstein duality** holds. Namely,

$$\inf_{\pi \in \Pi(\mu, \nu)} \sum_{x, y \in \mathcal{V}} d(x, y) \pi(x, y) = \sup_{f \in \text{Lip}_1(\mathcal{V})} \sum f(z) (\mu - \nu), \quad (6)$$

where $\pi \in \Pi(\mu, \nu)$ is a coupling between μ, ν and $f : \mathcal{V} \mapsto \mathbb{R} \in \text{Lip}_1(\mathcal{V})$, if for all $x, y \in \mathcal{V}$, $f(y) - f(x) \leq d(x, y)$.

Proof of Theorem 3.4 is given in Appendix A.6. Additionally, for computational intensive scenario, we offer two lower-bound estimations of CURC under distinct assumptions in Appendix A.26 and A.29, with computational costs of $\mathcal{O}(n^3)$ and $\mathcal{O}(n^4)$, respectively. Here, we define the **reciprocal edge weight** to construct such **asymmetric distance function**.

Definition 3.5. (Reciprocal edge weight) Let ε be a small positive real value, then the ε -masked reciprocal edge weight $\mathbf{r}^\varepsilon : \mathcal{V} \times \mathcal{V} \mapsto \mathbb{R}^{>0} \cup \{\infty\}$ is defined by

$$\mathbf{r}^\varepsilon(x, y) := \begin{cases} \frac{1}{\omega(x, y)} & \text{if } \omega(x, y) \geq \varepsilon \\ \frac{1}{\varepsilon} & \text{if } \omega(x, y) < \varepsilon \end{cases}$$

Definition 3.6. (Reciprocal distance function) The ε -masked reciprocal distance function $d^\varepsilon : \mathcal{V} \times \mathcal{V} \mapsto \mathbb{R}^{>0} \cup \{\infty\}$ is defined by

$$d^\varepsilon := \text{shortest path with } \mathbf{r}^\varepsilon \text{ as edge length.}$$

In particular, d^ϵ is a possibly **asymmetric distance function** on $\mathcal{V} \times \mathcal{V}$, which is consistent with directed-weighted graph propagation in GPNNs. Now we are ready to drive the definition of CURC. Attention should be placed to handle the singularity issue of reciprocal distance. We use an extra definition with κ_{CURC}^ϵ to define κ_{CURC} with ϵ limit.

Definition 3.7. (CURC) Let $\mathcal{G} = (\mathcal{V}, \mathcal{E}, \omega)$ be a graph equipped with the ϵ -masked weighted reciprocal distance function d^ϵ . For distinct $x, y \in \mathcal{V}$, we define the ϵ -masked Continuous Unified Ricci Curvature by

$$\kappa_{CURC}^\epsilon(x, y) := 1 - \frac{\mathcal{W}_1^\epsilon(\mu_x, \mu_y)}{d^\epsilon(x, y)},$$

where the Wasserstein distance \mathcal{W}_1^ϵ is based on d^ϵ . The corresponding *Continuous Unified Ricci Curvature (CURC)* is defined by

$$\kappa_{CURC}(x, y) := \lim_{\epsilon \rightarrow 0} \kappa_{CURC}^\epsilon(x, y).$$

3.3 Optimal Transport of Information

Here, we share intuition over optimal transport of information. Existing application of optimal transportation in a message-passing on graphs $G = (\mathcal{V}, \mathcal{E})$ is investigated by [Topping et al., 2022], utilizing Ollivier-Ricci (OR) curvature. For vertices x, y , OR-curvature, represented as $\kappa_{OR}(x, y)$, evaluates the ratio of Wasserstein to graph distance, signifying the cost of moving uniform mass across edges. In this framework, information from each vertex x diminishes as it spreads to neighboring vertices due to the nested aggregation function. Such diminishing impact is akin to the cost in Wasserstein distance. By normalizing this, we assert OR-curvature as a metric to measure the difficulty of information transport between vertices. This motivates us to develop CURC based on optimal transport.

3.4 Properties of CURC

Proposition 3.8. *The Continuous Unified Ricci Curvature κ_{CURC} admits the following properties:*

- (Unity) For connected unweighted-undirected graph $\mathcal{G} = (\mathcal{V}, \mathcal{E})$, for any vertex pair $x, y \in \mathcal{V}$, we have $\kappa_{CURC}(x, y) = \kappa_{OR}(x, y)$, where κ_{OR} is the Ollivier-ricci curvature.
- (Continuity) If we perceive $\kappa_{CURC}(x, y)$ as a function of ω , then $\kappa_{CURC}(x, y)$ is continuous w.r.t. ω entry-wise.
- (Scale invariance) For strongly-connected weighted-directed graph $\mathcal{G} = (\mathcal{V}, \mathcal{E}, \omega)$, when all edge weights ω are scaled by an arbitrary positive constant λ , the value of $\kappa_{CURC}(x, y)$ for any vertex pair $x, y \in \mathcal{V}$ is invariant.

Detailed proof Proposition 3.8 is given in Appendix A.14. The Unity and Continuity properties collectively establish CURC as a continuous extension of the canonical Ollivier-Ricci curvature, as originally introduced in Ollivier [2009]. Scale invariance is a crucial property for CURC being a measure of bottlenecks on the propagation graph. Intuitively, uniformly scaling of edge weight does not change the dynamics of information on the propagation graph, leading to a robust bottlenecks or oversquashing measure on the graph.

Furthermore, we establish how CURC can be perceived as a measure of bottlenecks phenomenon with the help of the so-called *Dirichlet isoperimetric constant*, which is the direct extension of *Cheeger constant* into strongly-connected weighted-directed graphs. *Cheeger constant* has been widely used to measure bottlenecks of GNN message-passing on undirected-unweighted graphs due to its connection with community clustering. In Topping et al. [2022], they established the connection between Balanced Forman curvature with Cheeger constant using spectral properties. Likewise, we derive similar property between CURC and Dirichlet isoperimetric constant to conclude our theoretical discussion of CURC and its connection to bottlenecks.

Definition 3.9. (Boundary Perron-measure) For a non-empty $\Omega \subset \mathcal{V}$, its *Boundary Perron-measure* is defined as

$$\mathbf{m}(\partial\Omega) := \sum_{y \in \Omega} \sum_{z \in \mathcal{V} \setminus \Omega} \mathbf{m}_{yz},$$

where $\mathbf{m}_{yz} := \mathbf{m}(y)\mu(y, z)$ and $\mathbf{m}(\Omega) = \sum_{x \in \Omega} \mathbf{m}(x)$.

Definition 3.10. (Dirichlet isoperimetric constant) The *Dirichlet isoperimetric constant* $\mathcal{I}_{\mathcal{V}}^D$ on a non-empty set \mathcal{V} is defined by

$$\mathcal{I}_{\mathcal{V}}^D := \inf_{\Omega \subset \mathcal{V}} \frac{\mathbf{m}(\partial\Omega)}{\mathbf{m}(\Omega)}.$$

Theorem 3.11. *Let $\mathcal{G} = (\mathcal{V}, \mathcal{E}, \omega)$ and $E_R(x) := \{y \in \mathcal{V} \mid d(x, y) \geq R\}$. Fix $x \in \mathcal{V}$, we assume $\inf_{y \in \mathcal{V} \setminus \{x\}} \kappa_{\text{CURC}}(x, y) \geq K$ for some $K \in \mathbb{R}$ and $-\sum_{y \in \mathcal{V}} \mu(x, y)d(x, y) \geq \Lambda$ for some $\Lambda \in (-\infty, 0)$. For $D > 0$, we further assume that for all $y \in \mathcal{V}$, $d(x, y) \leq D$. Then the Dirichlet isoperimetric constant admits the following lower bound:*

$$\mathcal{I}_{E_R(x)}^D \geq \frac{KR + \Lambda}{D}.$$

Proof of Theorem 3.11 is given in Appendix A.25. Same as its counterpart in undirected-unweighted graphs, a small Dirichlet isoperimetric constant indicates higher probability of bottlenecks on propagation graph. For a fixed vertex x , a large value of $\kappa_{\text{CURC}}(x, y)$ for $y \in \mathcal{V}$ implies a large value of K , which results in a larger lower bound for the Dirichlet isoperimetric constant $\mathcal{I}_{E_R(x)}^D$ according to Theorem 3.11. Combined with Proposition 3.8, CURC constitutes a proper instrument for measuring the bottleneck phenomenon on propagation graphs within our GPNN framework. For better visualization, we present the CURC distributions of our GPNN models in the later experiments.

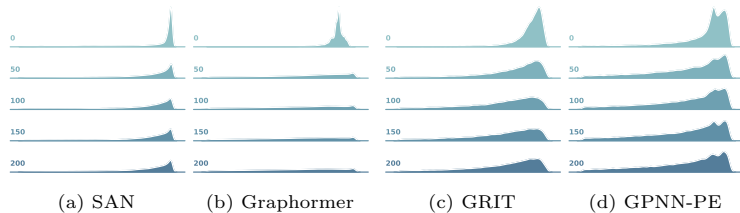


Figure 3: Visualization of the curvature distribution characterized on ZINC for 4 models with dynamic propagation learned from data. The CURC distribution of 0 to 200 epochs are placed vertically for each model. A tendency of curvature shifting to their left side is observed across all models. This ubiquitous *decurve flow* phenomenon suggests a change of bottlenecks by the directed-unweighted propagation graphs analysis central to this work.

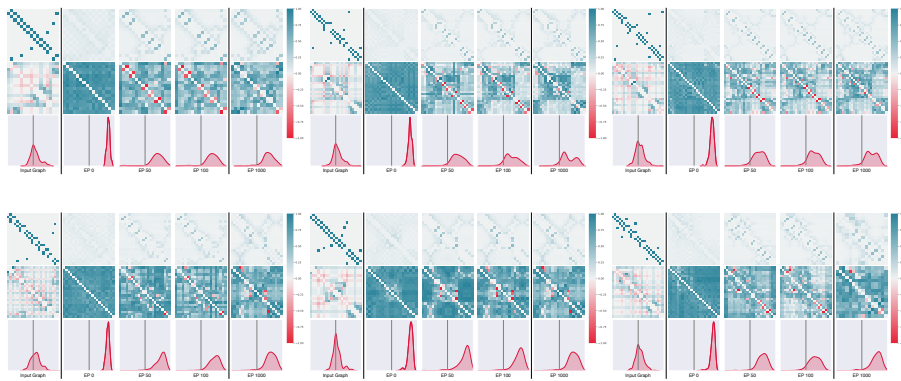


Figure 4: Visualization of Generalized Propagation and its Curvature for 6 graphs in ZINC at . 1st row: the visualization of propagation graph connection ω_{uv} ; 2nd row: the visualization of CURC $\kappa_{CURC}(u, v)$; 3rd row: the distributions of CURC; In the left most column, we visualize the input graph. Ep-0, Ep-50, Ep-100, Ep-1000 are listed afterwards.

4 “Decurve Flow” Phenomenon

The proposed Continuous Unified Ricci Curvature (CURC) allows for in-depth analysis of geometric properties in GPNN variants, particularly focusing on Graph Transformers (GTs). This analysis aids in identifying optimal propagation graph structures, enhancing our understanding of graph learning and informing the design of new GPNN models.

4.1 Analyzing the Learning Dynamic on CURC

To better understand the behavior of GTs and exploring potential learning patterns, we analyze the trend in CURC distributions of the propagation graphs

during training.

We consider three classical graph transformers, Graphormer [Ying et al., 2021], SANs [Kreuzer et al., 2021b], GRIT [Ma et al., 2023] as well as a simplified, *feat. ind.* variant of GRIT, namely GPNN-PE (details in Appx. F.1).

We first visualize the kernel density estimate (KDE) plots of CURC distributions on sampled graphs from ZINC datasets on 0, 50, 100, 150 and 200 training epochs (as shown in Fig. 3). Based on the visualization, we reveal that these models all exhibit similar learning patterns: the propagation graphs at the initial stage resemble a smoothed complete graph resulting in a strongly right-skewed CURC distribution with nearly all positive curvatures. As the training epochs increase, the learned propagation graphs gradually shift towards the left, indicating the geometric patterns learned from the graphs.

We name this phenomenon as *decurve flow*. In fact, *Decurve flow* can be connected to the recent study on the relationship between over-smoothing and over-squashing [Giraldo et al., 2022]. Giraldo et al. [2022] reveal that small curvature values might cause the over-squashing problem, whereas, over-large curvatures might, on the other hand, lead to over-smoothing issues. Correspondingly, we conjecture that, even though start with random initialized complete propagation graphs, GTs learn to diminish the CURC to alleviate over-smoothing. In other words, there might exist an optimal propagation graph, balancing the over-squashing and over-smoothing, which is potentially identifiable via further in-depth analysis on the CURC distributions.

4.2 In-depth exploration on propagation matrices, CURC maps and CURC distributions

To further understand *decurve flow*, we go beyond the distribution and visualize propagation matrices (1st row), the corresponding CURC maps (2nd row) as well as the CURC distributions (3rd row) of GPNN-PE on 6 graphs from ZINC (shown in Fig 4). From the visualization, we observe that the CURC maps of GPNN-PE, from all large positive values, gradually learn small and even negative CURC values for certain node pairs. These observations match our conjecture: a well-optimized propagation matrix might deliberately diminish the information transport between two nodes, in order to prevent over-smoothing.

5 Navigating GPNN Design

GPNN framework unifies GTs, MPNNs and their variants by two key components, *adjacency function* and *connectivity function*. Here, we first conduct a series of in-depth exploratory experiments on ZINC datasets [Dwivedi et al., 2022a] to explore their design spaces and reveal the effective configurations as well as ineffective ones. Then we conduct thorough experiments on five datasets from [Dwivedi et al., 2022a] and two from [Dwivedi et al., 2022b] to properly justify our hypothesis on the configurations.

5.1 Designs of Connectivity Functions

In Sec.2.1, we discuss the taxonomy of the connectivity functions in our GPNN framework. Here, we explore the impact of each potential design on the connectivity functions and identify the essential configurations. Here, we conduct a thorough comparison experiment on ZINC-12K [Dwivedi et al., 2022a] for different variants of GPNNs with different configurations: (1) *feat. dep.* ✓v.s., *feat. ind.* ✗; (2) *dynamic* ✓v.s. *static* ✗; (3) *multi-head* ✓v.s. *single head* ✗; as well as (4) *global* ✓v.s. *local* ✗; The experimental results are shown in Table 1.

Empirically, compared to the full configuration (all ✓), changing *feat. dep.* to *feat. ind.* only leads to a statistically insignificant performance drop. This empirical finding matches our theoretical analysis in Sec. 2.2: the adjacency function is the dominant component of the expressive power on distinguishing non-isomorphism graphs, whereas the *feat. ind.* counterpart is much less essential. This drives us to conduct further ablation study based on this variant. From the empirical results, changing *global* to *local*, *dynamic* to *static* and *multi-head* to *single-head* will demonstrate different levels of decline in efficacy. The comparisons against two existing MPNNs demonstrate similar findings and also hint the importantness of the choices of adjacency functions.

Table 1: The Exploration of Connectivity Function

ZINC (MAE↓)	Local✗ Global✓	Static✗ Dynamic✓	Single ✗ Multi. ✓ Head.	Feat. Ind. ✗ Cond. ✓	Adj. Func.	Model
0.059 ± 0.002	✓	✓	✓	✓	21-RRWP*	GRIT
0.060 ± 0.003	✓	✓	✓	✗	21-RRWP	GPNN-PE
0.064 ± 0.002	✓	✗	✓	✗	21-RRWP	+ static
0.066 ± 0.005	✓	✓	✗	✗	21-RRWP	+ 1-head
0.068 ± 0.003	✗	✓	✓	✗	21-RRWP	+ local
0.070 ± 0.004	✗	✗	✗	✗	RWSE+1-RRWP	(GINE+RWSE)
0.526 ± 0.051	✗	✗	✗	✗	1-RRWP	(GIN)

*: 21-RRWP will naturally include RWSE with 21-order.

Table 2: Adjacency Function; For absolute PE $\hat{\mathbf{P}}_i$, we retain the usage as absolute PE $\mathbf{P}_{i,i}$ as well as concatenate them $\mathbf{P}_{i,j} = [\hat{\mathbf{P}}_i, \hat{\mathbf{P}}_j]$ to construct relative PE

Adjacency Function	ZINC (MAE↓)
21-RRWP	0.060 ± 0.003
SPD	0.072 ± 0.004
pair-LapPE	0.151 ± 0.006
1-RRWP	0.125 ± 0.006

5.2 Designs of Adjacency Function

Following the previous exploration, we would like to verify the essentiality of the adjacency function on the empirical results. Specifically, using GPNN-PE as the platform for comparison, we conduct experiments on ZINC, comparing 4 choices

of adjacency function designs: 21-order RRWP (more details in Appendix F.1.2)), paired Laplacian Positional encoding (pair-LapPE), 1-order RRWP (equivalent to random matrix plus self-identification), and shortest-path distance [Ying et al., 2021] (as shown in Tab. 2). The experimental results are shown in Table 2. According to the empirical results, GPNN-PEs with different choices of adjacency functions demonstrate huge performance differences, revealing the importance of the design choices on the adjacency functions.

5.3 Benchmarking GPNN-PE

To verify our findings in the previous exploratory experiments, we would like to further benchmark our highlighted GPNN variant, GPNN-PE, in comparison to other typical graph models. Thus, we further evaluate GPNN-PE on two datasets from the Long-Range Graph Benchmark (LRGB) [Dwivedi et al., 2022b] (shown in Tab. 3). The empirical results further justify our theoretical findings: GPNN-PE reaches a comparable performance to GRIT and outperforms other GTs and MPNNs with weaker adjacency functions. More experimental results and further details concerning the experimental setup can be found in Appendix F.2.

Table 3: Test performance on LRGB [Dwivedi et al., 2022b]. Shown is the mean \pm s.d. of 4 runs. Highlighted are the top **first**, **second**, and **third** results. # Param \sim 500K.

Model	Peptides-func	Peptides-struct
	AP \uparrow	MAE \downarrow
GCN	0.5930 \pm 0.0023	0.3496 \pm 0.0013
GINE	0.5498 \pm 0.0079	0.3547 \pm 0.0045
GatedGCN	0.5864 \pm 0.0035	0.3420 \pm 0.0013
GatedGCN+RWSE	0.6069 \pm 0.0035	0.3357 \pm 0.0006
Transf.+LapPE	0.6326 \pm 0.0126	0.2529 \pm 0.0016
SAN+LapPE	0.6384 \pm 0.0121	0.2683 \pm 0.0043
SAN+RWSE	0.6439 \pm 0.0075	0.2545 \pm 0.0012
GPS	0.6535 \pm 0.0041	0.2500 \pm 0.0012
GRIT	0.6988 \pm 0.0082	0.2460 \pm 0.0012
GPNN-PE	0.6954 \pm 0.0023	0.2474 \pm 0.0010

6 Conclusion and Future Work

This study addresses the limitations of the traditional analysis of message-passing, central to graph learning, by defining generalized propagation with directed and weighted graphs. The introduced Generalized Propagation Networks (GPNNs) unifies Graph Transformers (GTs), Message Passing Neural Networks (MPNNs), and their variants through the use of directed, weighted propagation graphs. This approach aims to advance the field by incorporating "attention" mechanisms into graph analysis, which have been largely overlooked in traditional, undirected, and unweighted graph models. Our findings demonstrate that the expressiveness

of GPNNs is fundamentally tied to the design of the adjacency function, thereby highlighting its theoretical and practical importance. Additionally, we have presented a taxonomy for GPNN-related models, illuminating the prevalent design choices and their implications through empirical analysis within this framework. Furthermore, we proposed the Continuous Unified Ricci Curvature (CURC), an extension of the Ollivier-Ricci (OR) Curvature, tailored for directed and weighted graphs. The CURC exhibits key properties such as continuity, unity with OR curvature under specific conditions, and a novel lower bound relationship with the Dirichlet Isoperimetric Constant, facilitating enhanced analysis of graph bottlenecks. By CURC, we reveal the “*decurve flow*” phenomenon, calling for future research with propagation analysis on weighted-directed graphs.

References

- Will Hamilton, Zhitao Ying, and Jure Leskovec. Inductive Representation Learning on Large Graphs. In *Adv. Neural Inf. Process. Syst.*, volume 30. Curran Associates, Inc., 2017.
- Petar Veličković, Guillem Cucurull, Arantxa Casanova, Adriana Romero, Pietro Liò, and Yoshua Bengio. Graph Attention Networks. In *Proc. Int. Conf. Learn. Representations*, February 2018.
- Federico Monti, Davide Boscaini, Jonathan Masci, Emanuele Rodolà, Jan Svoboda, and Michael M. Bronstein. Geometric deep learning on graphs and manifolds using mixture model CNNs. In *IEEE Conference on Computer Vision and Pattern Recognition (CVPR)*, 2017.
- Keyulu Xu, Weihua Hu, Jure Leskovec, and Stefanie Jegelka. How Powerful are Graph Neural Networks? In *Proc. Int. Conf. Learn. Representations*, February 2019.
- Zhengdao Chen, Soledad Villar, Lei Chen, and Joan Bruna. On the equivalence between graph isomorphism testing and function approximation with GNNs. In *Adv. Neural Inf. Process. Syst.*, pages 15894–15902, Red Hook, NY, USA, December 2019. Curran Associates Inc.
- Uri Alon and Eran Yahav. On the bottleneck of graph neural networks and its practical implications. *arXiv preprint arXiv:2006.05205*, 2020.
- Deli Chen, Yankai Lin, Wei Li, Peng Li, Jie Zhou, and Xu Sun. Measuring and relieving the over-smoothing problem for graph neural networks from the topological view. In *Proceedings of the AAAI conference on artificial intelligence*, volume 34, pages 3438–3445, 2020.
- Kenta Oono and Taiji Suzuki. Graph neural networks exponentially lose expressive power for node classification. *arXiv preprint arXiv:1905.10947*, 2019.
- Ashish Vaswani, Noam Shazeer, Niki Parmar, Jakob Uszkoreit, Llion Jones, Aidan N Gomez, Lukasz Kaiser, and Illia Polosukhin. Attention is all you need. In *NeurIPS*, 2017.
- Vijay Prakash Dwivedi and Xavier Bresson. A Generalization of Transformer Networks to Graphs. In *Proc. AAAI Workshop Deep Learn. Graphs: Methods Appl.*, January 2021.
- Devin Kreuzer, Dominique Beaini, William L. Hamilton, Vincent Létourneau, and Prudencio Tossou. Rethinking Graph Transformers with Spectral Attention. In *Adv. Neural Inf. Process. Syst.*, May 2021a.
- Ladislav Rampásek, Mikhail Galkin, Vijay Prakash Dwivedi, Anh Tuan Luu, Guy Wolf, and Dominique Beaini. Recipe for a General, Powerful, Scalable Graph Transformer. In *Adv. Neural Inf. Process. Syst.*, May 2022.

- Dexiong Chen, Leslie O’Bray, and Karsten Borgwardt. Structure-Aware Transformer for Graph Representation Learning. In *Proc. Int. Conf. Mach. Learn.*, pages 3469–3489, June 2022.
- Liheng Ma, Chen Lin, Derek Lim, Adriana Romero-Soriano, Puneet K Dokania, Mark Coates, Philip Torr, and Ser-Nam Lim. Graph inductive biases in transformers without message passing. *arXiv preprint arXiv:2305.17589*, 2023.
- Chen Cai, Truong Son Hy, Rose Yu, and Yusu Wang. On the Connection Between MPNN and Graph Transformer. In *Proc. Int. Conf. Mach. Learn.* arXiv, 2023. URL <http://arxiv.org/abs/2301.11956>. arXiv:2301.11956 [cs].
- Hamed Shirzad, Ameya Velingker, Balaji Venkatachalam, Danica J Sutherland, and Ali Kemal Sinop. Exphormer: Sparse transformers for graphs. *arXiv preprint arXiv:2303.06147*, 2023a.
- Jhony H Giraldo, Fragkiskos D Malliaros, and Thierry Bouwmans. Understanding the relationship between over-smoothing and over-squashing in graph neural networks. *arXiv preprint arXiv:2212.02374*, 2022.
- Yann Ollivier. Ricci curvature of markov chains on metric spaces. *Journal of Functional Analysis*, 256(3):810–864, 2009.
- Jake Topping, Francesco Di Giovanni, Benjamin Paul Chamberlain, Xiaowen Dong, and Michael M. Bronstein. Understanding over-squashing and bottlenecks on graphs via curvature. In *Proc. Int. Conf. Learn. Representations*, March 2022.
- Thomas N. Kipf and Max Welling. Semi-Supervised Classification with Graph Convolutional Networks. In *Proc. Int. Conf. Learn. Representations*, 2017.
- Xavier Bresson and Thomas Laurent. Residual Gated Graph ConvNets. *arXiv*, April 2018.
- Michaël Defferrard, Xavier Bresson, and Pierre Vandergheynst. Convolutional Neural Networks on Graphs with Fast Localized Spectral Filtering. In *Adv. Neural Inf. Process. Syst.*, 2016.
- Johannes Gasteiger, Stefan Weiß enberger, and Stephan Günnemann. Diffusion Improves Graph Learning. In *Adv. Neural Inf. Process. Syst.*, volume 32. Curran Associates, Inc., 2019.
- Fabrizio Frasca, Emanuele Rossi, Davide Eynard, Ben Chamberlain, Michael Bronstein, and Federico Monti. SIGN: Scalable Inception Graph Neural Networks. In *arXiv:2004.11198 [Cs, Stat]*, November 2020.
- Md Shamim Hussain, Mohammed J. Zaki, and Dharmashankar Subramanian. Global Self-Attention as a Replacement for Graph Convolution. In *Proc. ACM SIGKDD Int. Conf. Knowl Discov. Data Min. (KDD)*, August 2022. doi: 10.1145/3534678.3539296.

- Ryunosuke Ozawa, Yohei Sakurai, and Taiki Yamada. Geometric and spectral properties of directed graphs under a lower ricci curvature bound. *Calculus of Variations and Partial Differential Equations*, 59:1–39, 2020.
- Yong Lin, Linyuan Lu, and Shing-Tung Yau. Ricci curvature of graphs. *Tohoku Mathematical Journal, Second Series*, 63(4):605–627, 2011.
- James R. Kirkwood and Bessie H. Kirkwood. The perron–frobenius theorem. *Linear Algebra*, 2020. URL <https://api.semanticscholar.org/CorpusID:120536925>.
- Chengxuan Ying, Tianle Cai, Shengjie Luo, Shuxin Zheng, Guolin Ke, Di He, Yanming Shen, and Tie-Yan Liu. Do Transformers Really Perform Badly for Graph Representation? In *Adv. Neural Inf. Process. Syst.*, 2021.
- Devin Kreuzer, Dominique Beaini, Will Hamilton, Vincent Létourneau, and Prudencio Tossou. Rethinking graph transformers with spectral attention. *Advances in Neural Information Processing Systems*, 34:21618–21629, 2021b.
- Vijay Prakash Dwivedi, Chaitanya K. Joshi, Thomas Laurent, Yoshua Bengio, and Xavier Bresson. Benchmarking Graph Neural Networks. *J. Mach. Learn. Res.*, December 2022a.
- Vijay Prakash Dwivedi, Ladislav Rampásek, Mikhail Galkin, Ali Parviz, Guy Wolf, Anh Tuan Luu, and Dominique Beaini. Long Range Graph Benchmark. In *Adv. Neural Inf. Process. Syst.*, December 2022b.
- Peter D Lax. *Linear algebra and its applications*, volume 78. John Wiley & Sons, 2007.
- Alexander Grigor’yan. *Introduction to analysis on graphs*, volume 71. American Mathematical Soc., 2018.
- Jürgen Jost and Shiping Liu. Ollivier’s ricci curvature, local clustering and curvature-dimension inequalities on graphs. *Discrete & Computational Geometry*, 51(2):300–322, 2014.
- Christopher Morris, Martin Ritzert, Matthias Fey, William L. Hamilton, Jan Eric Lenssen, Gaurav Rattan, and Martin Grohe. Weisfeiler and Leman Go Neural: Higher-Order Graph Neural Networks. In *Proc. AAAI Conf. Artif. Intell.*, volume 33, pages 4602–4609, July 2019a. doi: 10.1609/aaai.v33i01.33014602.
- Kurt Hornik, Maxwell Stinchcombe, and Halbert White. Multilayer feedforward networks are universal approximators. *Neural Netw.*, 2(5):359–366, 1989.
- Bohang Zhang, Shengjie Luo, Liwei Wang, and Di He. Rethinking the expressive power of GNNs via graph biconnectivity. In *Proc. Int. Conf. Learn. Representations*, 2023. URL <https://openreview.net/forum?id=r9hNv76KoT3>.

- Justin Gilmer, Samuel S. Schoenholz, Patrick F. Riley, Oriol Vinyals, and George E. Dahl. Neural Message Passing for Quantum Chemistry. In *Proc. Int. Conf. Mach. Learn.*, June 2017a.
- Justin Gilmer, Samuel S. Schoenholz, Patrick F. Riley, Oriol Vinyals, and George E. Dahl. Neural message passing for quantum chemistry, 2017b.
- B Yu Weisfeiler and A A Leman. The Reduction of a Graph to Canonical Form and the Algebra Which Appears Therein. *NTI, Series*, 2:12–16, 1968.
- Christopher Morris, Martin Ritzert, Matthias Fey, William L Hamilton, Jan Eric Lenssen, Gaurav Rattan, and Martin Grohe. Weisfeiler and leman go neural: Higher-order graph neural networks. In *Proceedings of the AAAI conference on artificial intelligence*, volume 33, pages 4602–4609, 2019b.
- Laszlo Babai and Ludik Kucera. Canonical labelling of graphs in linear average time. In *20th Annual Symposium on Foundations of Computer Science (sfcs 1979)*, pages 39–46, 1979. doi: 10.1109/SFCS.1979.8.
- Haggai Maron, Heli Ben-Hamu, Hadar Serviansky, and Yaron Lipman. Provably Powerful Graph Networks. In *Advances in Neural Information Processing Systems*, volume 32. Curran Associates, Inc., 2019.
- Christopher Morris, Gaurav Rattan, Sandra Kiefer, and Siamak Ravanbakhsh. Speqnets: Sparsity-aware permutation-equivariant graph networks. In *International Conference on Machine Learning*, pages 16017–16042. PMLR, 2022.
- Fabrizio Frasca, Beatrice Bevilacqua, Michael Bronstein, and Haggai Maron. Understanding and extending subgraph gnns by rethinking their symmetries. *Advances in Neural Information Processing Systems*, 35:31376–31390, 2022.
- Beatrice Bevilacqua, Fabrizio Frasca, Derek Lim, Balasubramanian Srinivasan, Chen Cai, Gopinath Balamurugan, Michael M. Bronstein, and Haggai Maron. Equivariant Subgraph Aggregation Networks. In *Proc. Int. Conf. Learn. Representations*, March 2022.
- Pascal Welke, Maximilian Thiessen, Fabian Jögl, and Thomas Gärtner. Expectation-complete graph representations with homomorphisms. *arXiv preprint arXiv:2306.05838*, 2023.
- Omri Puny, Derek Lim, Bobak Kiani, Haggai Maron, and Yaron Lipman. Equivariant polynomials for graph neural networks. In *International Conference on Machine Learning*, pages 28191–28222. PMLR, 2023.
- Lingxiao Zhao and Leman Akoglu. PairNorm: Tackling Oversmoothing in Gnns. In *International Conference on Learning Representations (ICLR)*, page 17, 2020.

- Frederik Wenkel, Yimeng Min, Matthew Hirn, Michael Perlmutter, and Guy Wolf. Overcoming Oversmoothness in Graph Convolutional Networks via Hybrid Scattering Networks, August 2022.
- Benjamin Gutteridge, Xiaowen Dong, Michael M Bronstein, and Francesco Di Giovanni. Drew: Dynamically rewired message passing with delay. In *International Conference on Machine Learning*, pages 12252–12267. PMLR, 2023.
- Rickard Brüel-Gabrielsson, Mikhail Yurochkin, and Justin Solomon. Rewiring with positional encodings for graph neural networks. *arXiv preprint arXiv:2201.12674*, 2022.
- Ziwei Zhang, Peng Cui, Jian Pei, Xin Wang, and Wenwu Zhu. Eigen-GNN: A Graph Structure Preserving Plug-in for GNNs. *IEEE Trans. Knowl. Data Eng.*, pages 1–1, 2021. ISSN 1558-2191. doi: 10.1109/TKDE.2021.3112746.
- Derek Lim, Joshua David Robinson, Lingxiao Zhao, Tess Smidt, Suvrit Sra, Haggai Maron, and Stefanie Jegelka. Sign and Basis Invariant Networks for Spectral Graph Representation Learning. In *Proc. Int. Conf. Learn. Representations*, 2023.
- Haorui Wang, Haoteng Yin, Muhan Zhang, and Pan Li. Equivariant and Stable Positional Encoding for More Powerful Graph Neural Networks. In *Proc. Int. Conf. Learn. Representations*, May 2022.
- Vijay Prakash Dwivedi, Anh Tuan Luu, Thomas Laurent, Yoshua Bengio, and Xavier Bresson. Graph Neural Networks with Learnable Structural and Positional Representations. In *Proc. Int. Conf. Learn. Representations*, September 2021.
- Giorgos Bouritsas, Fabrizio Frasca, Stefanos Zafeiriou, and Michael M Bronstein. Improving graph neural network expressivity via subgraph isomorphism counting. *IEEE Transactions on Pattern Analysis and Machine Intelligence*, 45(1): 657–668, 2022a.
- Ameya Velingker, Ali Kemal Sinop, Ira Ktena, Petar Veličković, and Sreenivas Gollapudi. Affinity-Aware Graph Networks, June 2022.
- Jiaxuan You, Rex Ying, and Jure Leskovec. Position-aware Graph Neural Networks. In *Proc. Int. Conf. Mach. Learn.*, pages 7134–7143. PMLR, May 2019.
- Pan Li, Yanbang Wang, Hongwei Wang, and Jure Leskovec. Distance Encoding: Design Provably More Powerful Neural Networks for Graph Representation Learning. In *Adv. Neural Inf. Process. Syst.*, 2020.
- Cristian Bodnar, Fabrizio Frasca, Yuguang Wang, Nina Otter, Guido F. Montufar, Pietro Lió, and Michael Bronstein. Weisfeiler and Lehman Go Topological: Message Passing Simplicial Networks. In *Proc. Int. Conf. Mach. Learn.*, pages 1026–1037. PMLR, July 2021.

- Cai Zhou, Xiyuan Wang, and Muhan Zhang. From relational pooling to subgraph gns: A universal framework for more expressive graph neural networks. *arXiv preprint arXiv:2305.04963*, 2023.
- Shuliang Bai, Yong Lin, Linyuan Lu, Zhiyu Wang, and Shing-Tung Yau. Ollivier ricci-flow on weighted graphs. *arXiv preprint arXiv:2010.01802*, 2020.
- Federico Barbero, Ameya Velingker, Amin Saberi, Michael Bronstein, and Francesco Di Giovanni. Locality-aware graph-rewiring in gns. *arXiv preprint arXiv:2310.01668*, 2023.
- Federico Barbero, Cristian Bodnar, Haitz Sáez de Ocariz Borde, Michael Bronstein, Petar Veličković, and Pietro Liò. Sheaf Neural Networks with Connection Laplacians. In *Proc. Int. Conf. Mach. Learn. Workshop Topol. Algebra Geom. Mach. Learn.* arXiv, June 2022.
- Xiyuan Wang and Muhan Zhang. How Powerful are Spectral Graph Neural Networks. In *Proc. Int. Conf. Mach. Learn.*, pages 23341–23362. PMLR, June 2022.
- Jialin Zhao, Yuxiao Dong, Ming Ding, Evgeny Kharlamov, and Jie Tang. Adaptive Diffusion in Graph Neural Networks. In *Adv. Neural Inf. Process. Syst.*, volume 34, pages 23321–23333. Curran Associates, Inc., 2021a.
- Hamed Shirzad, Ameya Velingker, Balaji Venkatachalam, Danica J Sutherland, and Ali Kemal Sinop. Exphormer: Scaling Graph Transformers with Expander Graphs. In *Proc. Int. Conf. Mach. Learn.*, 2023b. URL <https://openreview.net/forum?id=8Tr3v4ueNd7>.
- Manzil Zaheer, Satwik Kottur, Siamak Ravanbakhsh, Barnabas Poczos, Russ R Salakhutdinov, and Alexander J Smola. Deep Sets. In *Adv. Neural Inf. Process. Syst.*, 2017.
- Joan Bruna, Wojciech Zaremba, Arthur Szlam, and Yann LeCun. Spectral Networks and Locally Connected Networks on Graphs. In *International Conference on Learning Representations (ICLR)*, May 2014.
- Deyu Bo, Chuan Shi, Lele Wang, and Renjie Liao. Specformer: Spectral Graph Neural Networks Meet Transformers. In *Proc. Int. Conf. Learn. Representations*, 2023. URL <https://openreview.net/forum?id=OpdSt3oyJa1>.
- Weihua Hu, Bowen Liu*, Joseph Gomes, Marinka Zitnik, Percy Liang, Vijay Pande, and Jure Leskovec. Strategies for Pre-training Graph Neural Networks. In *Proc. Int. Conf. Learn. Representations*, March 2020.
- Gabriele Corso, Luca Cavalleri, Dominique Beaini, Pietro Liò, and Petar Veličković. Principal Neighbourhood Aggregation for Graph Nets. In *Adv. Neural Inf. Process. Syst.*, December 2020.

- Shengjie Luo, Shanda Li, Shuxin Zheng, Tie-Yan Liu, Liwei Wang, and Di He. Your transformer may not be as powerful as you expect. In *Adv. Neural Inf. Process. Syst.*, 2022.
- Dominique Beani, Saro Passaro, Vincent Létourneau, Will Hamilton, Gabriele Corso, and Pietro Lió. Directional Graph Networks. In *Proc. Int. Conf. Mach. Learn.*, pages 748–758. PMLR, July 2021.
- Giorgos Bouritsas, Fabrizio Frasca, Stefanos P Zafeiriou, and Michael Bronstein. Improving Graph Neural Network Expressivity via Subgraph Isomorphism Counting. *IEEE Trans. Pattern Anal. Mach. Intell.*, pages 1–1, 2022b. ISSN 1939-3539. doi: 10.1109/TPAMI.2022.3154319.
- Jan Toenshoff, Martin Ritzert, Hinrikus Wolf, and Martin Grohe. Graph learning with 1d convolutions on random walks. *arXiv preprint arXiv:2102.08786*, 2021.
- Lingxiao Zhao, Wei Jin, Leman Akoglu, and Neil Shah. From stars to subgraphs: Uplifting any gnn with local structure awareness. In *Proc. Int. Conf. Learn. Representations*, 2021b.
- John J. Irwin, Teague Sterling, Michael M. Mysinger, Erin S. Bolstad, and Ryan G. Coleman. ZINC: A Free Tool to Discover Chemistry for Biology. *J. Chem. Inf. Model.*, 52(7):1757–1768, July 2012. ISSN 1549-9596. doi: 10.1021/ci3001277.
- Weihua Hu, Matthias Fey, Hongyu Ren, Maho Nakata, Yuxiao Dong, and Jure Leskovec. Ogb-lsc: A large-scale challenge for machine learning on graphs. In *Adv. Neural Inf. Process. Syst. Datasets Benchmarks Track*, 2021.

Appendices

A Detailed Proofs for CURC	24
A.1 Kantorovich-Rubinstein duality	24
A.2 Analytical and Algebraic Properties of Continuous Unified Ricci Curvature	28
A.3 Continuous Unified Ricci Curvature and Bottlenecking	33
B Expressiveness of GPNNs	40
B.1 Color refinement(CR)	40
B.2 Prototypical GPNNs	40
C Background	44
C.1 MPNNs	44
C.2 Graph Transformers	44
C.3 Expressiveness	44
C.4 Ollivier-Ricci Curvature	45
C.5 Over-squashing and over-smoothing Trade-off	46
C.6 Motivation for Unified Framework	46
D Related Works	47
E Generality of GPNN framework	48
E.1 Taxonomy of Existing Graph Models in GPNNs	48
E.2 Existing Models as GPNNs	48
F Experimental Details	52
F.1 Details of GPNN-PE	52
F.2 More about Experimental	53
F.3 Visualization of Curvature	54

A Detailed Proofs for CURC

A.1 Kantorovich-Rubinstein duality

Kantorovich-Rubinstein duality is an important result in the field of optimal transportation, which establishes the connection between optimal transportation problem and linear programming problem. The most common form of duality is stated in the context of Polish metric space. While in the setting up of κ_{CURC} , the distance function as weighted shortest distance is not necessarily symmetric, which fails to define a metric space. Luckily, the duality still holds under weaker assumption without symmetry assumption. Here, we give a short proof of Kantorovich-Rubinstein duality for the sake of completeness.

Definition A.1. (L-Lipschitz) Let $d : \mathcal{X} \times \mathcal{X} \mapsto \mathbb{R}^{\geq 0}$ be an asymmetric definite distance function on \mathcal{X} , we say $f : \mathcal{X} \mapsto \mathbb{R}$ is L-Lipschitz w.r.t. d if

$$\forall x, y \in \mathcal{X}, f(y) - f(x) \leq Ld(x, y).$$

Definition A.2. (Support) Let \mathcal{X} be a finite set and $\mu : \mathcal{X} \mapsto [0, 1]$ be the corresponding probability measure, we define the *support* of μ to be

$$\text{supp}(\mu) = \{x \in \mathcal{X} : \mu(x) > 0\}.$$

Definition A.3. (Coupling) Suppose μ and ν to be two probability distribution on finite sets \mathcal{X} and \mathcal{Y} respectively. Let $\Pi(\mu, \nu)$ denotes the set of *couplings* between μ and ν . We say $\pi : \mathcal{X} \times \mathcal{Y} \mapsto [0, 1] \in \Pi(\mu, \nu)$ is a *coupling* if

$$\sum_{y \in \mathcal{Y}} \pi(x, y) = \mu(x), \quad \sum_{x \in \mathcal{X}} \pi(x, y) = \nu(y).$$

Definition A.4. (C-convexity) Let \mathcal{X} and \mathcal{Y} be two sets and $c : \mathcal{X} \times \mathcal{Y} \mapsto \mathbb{R} \cup \{+\infty\}$. A function $f : \mathcal{X} \mapsto \mathbb{R} \cup \{+\infty\}$ is *c-convex* if it is not identically $+\infty$, and there exists $\psi : \mathcal{Y} \mapsto \mathbb{R} \cup \{+\infty\}$ such that

$$\forall x \in \mathcal{X}, f(x) = \sup_{y \in \mathcal{Y}} (\psi(y) - c(x, y)).$$

Then its corresponding *c-transform* is the function ψ^c defined by

$$\forall y \in \mathcal{Y}, f^c(y) = \inf_{x \in \mathcal{X}} (\psi(x) + c(x, y)).$$

Lemma A.5. Let $f : \mathcal{X} \mapsto \mathbb{R}$ be a function defined on a set \mathcal{X} . Let $d : \mathcal{X} \times \mathcal{X} \mapsto \mathbb{R}^{\geq 0}$ to be a distance function on \mathcal{X} that satisfies the following properties:

- $\forall x \in \mathcal{X}, d(x, x) = 0$
- $\forall x \neq y \in \mathcal{X}, d(x, y) > 0$
- $\forall x, y, z \in \mathcal{X}, d(x, z) + d(z, y) \geq d(x, y)$

Then function f is d -convex $\iff f$ is 1-Lipschitz w.r.t. distance function d .

Proof. We first suppose f is d -convex, we want to show that $\forall x, y \in \mathcal{X}, f(x) - f(y) \leq d(y, x)$. By the definition of c -convex, \exists function $\psi : \mathcal{X} \mapsto \mathbb{R}$, such that $f(x) = \sup_{z \in \mathcal{X}} [\psi(z) - d(x, z)]$ and $f(y) = \sup_{z \in \mathcal{X}} [\psi(z) - d(y, z)]$. Suppose $z_0 = \operatorname{argsup}_{z \in \mathcal{X}} [\psi(z) - d(x, z)]$

$$\begin{aligned} f(x) - f(y) &= \sup_{z \in \mathcal{X}} [\psi(z) - d(x, z)] - \sup_{z \in \mathcal{X}} [\psi(z) - d(y, z)] \\ &\leq [\psi(z_0) - d(x, z_0)] - [\psi(z_0) - d(y, z_0)] \\ &= d(y, z_0) - d(x, z_0) \\ &\leq d(y, x) \text{ by triangular inequality} \end{aligned}$$

Now, suppose f is 1-Lipschitz w.r.t. distance function d . We note that $f^c(y) = \inf_{x \in \mathcal{X}} [f(x) + d(x, y)]$. By 1-Lipschitz, we have that

$$\begin{aligned} f(y) - f(x) &\leq d(x, y) \\ \Rightarrow f(x) - f(y) &\geq -d(x, y) \\ \Rightarrow f(x) &\geq f(y) - d(x, y) \\ \Rightarrow f(x) &\geq \sup_{y \in \mathcal{X}} [f(y) - d(x, y)] \end{aligned}$$

by taking $x = y$ in the supremum and $d(x, x) = 0$, we have the following equality:

$$f(x) = \sup_{y \in \mathcal{X}} [f(y) - d(x, y)]$$

By the exact same argument, we can derive a bonus property that

$$f^c(y) = \inf_{x \in \mathcal{X}} [f(x) + d(x, y)] = f(y).$$

Therefore, on a set \mathcal{X} with asymmetric distance function that satisfies triangle inequality, function f is d -convexity $\iff f$ is 1-Lipschitz w.r.t. distance function d . And its c -transform is itself. \square

Theorem A.6. (*K-R duality*) Let \mathcal{V} be a discrete finite set equipped with a possibly asymmetric distance function $d : \mathcal{V} \times \mathcal{V} \mapsto \mathbb{R}^{\geq 0}$ that is definite and satisfies triangle inequality. Suppose μ and ν to be two probability measure on \mathcal{V} . Then we have the Kantorovich–Rubinstein duality:

$$\inf_{\pi \in \Pi(\mu, \nu)} \sum_{x, y \in \mathcal{V}} d(x, y) \pi(x, y) = \sup_{f \in \operatorname{Lip}(1)} \sum_{x \in \mathcal{V}} f(x) (\nu(x) - \mu(x)), \quad (1)$$

where $\Pi(\mu, \nu)$ denotes the coupling between probability measure μ and ν and $f \in \operatorname{Lip}(1)$ denotes that $f : \mathcal{V} \mapsto \mathbb{R}$ is 1-Lipschitz w.r.t. distance function d .

Proof. We prove equation 1 by first showing that

$$\inf_{\pi \in \Pi(\mu, \nu)} \sum_{x, y \in \mathcal{V}} d(x, y) \pi(x, y) \geq \sup_{f \in \operatorname{Lip}(1)} \sum_{x \in \mathcal{V}} f(x) (\nu(x) - \mu(x)). \quad (2)$$

Then we provide a specific construction of 1-Lipschitz function $f : \mathcal{V} \mapsto \mathbb{R}$ showing the converse,

$$\inf_{\pi \in \Pi(\mu, \nu)} \sum_{x, y \in \mathcal{V}} d(x, y) \pi(x, y) \leq \sup_{f \in \text{Lip}(1)} \sum_{x \in \mathcal{V}} f(x) (\nu(x) - \mu(x)). \quad (3)$$

Firstly, take arbitrary $\pi \in \Pi(\mu, \nu)$ and f 1-Lipschitz, we have the following algebraic property:

$$\begin{aligned} \sum_{x \in \mathcal{V}} f(x) (\nu(x) - \mu(x)) &= \sum_{x, y \in \mathcal{V}} f(x) \pi(x, y) - \sum_{x, y \in \mathcal{V}} f(y) \pi(x, y) \\ &= \sum_{x, y \in \mathcal{V}} [f(x) - f(y)] \pi(x, y) \\ &\leq \sum_{x, y \in \mathcal{V}} d(x, y) \pi(x, y) \end{aligned}$$

Therefore,

$$\begin{aligned} \inf_{\pi \in \Pi(\mu, \nu)} \sum_{x, y \in \mathcal{V}} d(x, y) \pi(x, y) &\geq \sum_{x \in \mathcal{V}} f(x) (\nu(x) - \mu(x)) \\ \Rightarrow \inf_{\pi \in \Pi(\mu, \nu)} \sum_{x, y \in \mathcal{V}} d(x, y) \pi(x, y) &\geq \sup_{f \in \text{Lip}(1)} \sum_{x \in \mathcal{V}} f(x) (\nu(x) - \mu(x)), \end{aligned}$$

which is exactly equation 2.

Secondly, we construct a function with the help of *c-convexity* introduced in definition A.4. For a fixed $m \in \mathbb{N}$, we can pick a sequence $(x_i, y_i)_{i=0}^m \in \text{supp}(\pi)$. Note that this choice of m is finite and $m \leq |\mathcal{V}|^2$. We construct our function f by

$$f(x) := \sup_{m \in \mathbb{N}} \sup_{(x_i, y_i)_{i=0}^m} \left\{ \sum_{i=0}^{m-1} [d(x_i, y_i) - d(x_{i+1}, y_i)] + [d(x_m, y_m) - d(x, y_m)] \right\}. \quad (4)$$

We now want to show that $f^c(y) - f(x) = d(x, y)$ almost surely for $(x, y) \in \text{supp}(\pi)$. Note that

$$\begin{aligned} f^c(y) &= \inf_{x \in \mathcal{X}} [f(x) + d(x, y)] \\ \Rightarrow f^c(y) &\leq f(x) + d(x, y) \\ \Rightarrow f^c(y) - f(x) &\leq d(x, y). \end{aligned}$$

By lemma A.5, we have that $f^c(y) = f(y)$, which implies that this choice of f guarantees 1-Lipschitz.

Suppose $(x, y) \in \text{supp}(\pi)$, and in the choice of sequence $(x_i, y_i)_{i=0}^m$ we can let

$(x_m, y_m) := (x, y)$. Therefore,

$$\begin{aligned} f(z) &\geq \sup_{m \in \mathbb{N}} \sup_{(x_i, y_i)_{i=0}^m} \left\{ \sum_{i=0}^{m-2} [d(x_i, y_i) - d(x_{i+1}, y_{i+1})] + [d(x_{m-1}, y_{m-1}) - d(x, y_{m-1})] \right. \\ &\quad \left. + [d(x, y) - d(z, y)] \right\} \\ &= f(x) + d(x, y) - d(z, y). \end{aligned}$$

The last equality comes from the fact that in the definition of f , taking supremum over m or $m - 1$ does not matter. Hence,

$$\begin{aligned} f(z) + d(z, y) &\geq f(x) + d(x, y) \\ \Rightarrow \inf_{z \in \mathcal{V}} [f(z) + d(z, y)] &\geq f(x) + d(x, y) \\ \Rightarrow f^c(y) &\geq f(x) + d(x, y) \\ \Rightarrow f^c(y) - f(x) &\geq d(x, y) \end{aligned}$$

Therefore, we have that $\forall (x, y) \in \text{supp}(\pi)$, $f^c(y) - f(x) = d(x, y) \iff f(y) - f(x) = d(x, y)$ by using lemma A.5 again. For clarity, we will denote this choice of f to be f^* . Using this result, we have $\forall \pi \in \Pi(\mu, \nu)$,

$$\begin{aligned} \sup_{f \in \text{Lip}(1)} \sum_{x \in \mathcal{V}} f(x) (\nu(x) - \mu(x)) &\geq \sum_{x \in \mathcal{V}} f^*(x) (\nu(x) - \mu(x)) \\ &= \sum_{x, y \in \mathcal{V}} [f^*(y) - f^*(x)] \pi(x, y) \\ &= \sum_{x, y \in \mathcal{V}} d(x, y) \pi(x, y) \\ &\geq \inf_{\pi \in \Pi(\mu, \nu)} \sum_{x, y \in \mathcal{V}} d(x, y) \pi(x, y) \end{aligned}$$

Therefore, both equations 2 and 3 hold, hence we have proven the Kantorovich–Rubinstein duality under the weaker assumption that distance function $d : \mathcal{V} \times \mathcal{V} \mapsto \mathbb{R}^{\geq 0}$ is not necessarily symmetric. \square

Corollary A.7. *Suppose \mathcal{V} to be a discrete finite set equipped with a possibly asymmetric distance function $d : \mathcal{V} \times \mathcal{V} \mapsto \mathbb{R}^{\geq 0}$ that satisfies triangle inequality. Suppose μ and ν to be two probability measure on \mathcal{V} with support on $\{x_1, x_2, \dots, x_n\}$ and $\{y_1, y_2, \dots, y_m\}$ respectively. Then solving the Wasserstein distance $\mathcal{W}_1(\mu, \nu) = \inf_{\pi \in \Pi(\mu, \nu)} \sum_{x, y \in \mathcal{V}} d(x, y) \pi(x, y)$ is equivalent with*

$$W_1(\mu, \nu) = \sup_{f \in \text{Lip}(1)} \left\{ \sum_i f(x_i) \nu(x_i) - \sum_j f(y_j) \mu(y_j) \right\}, \quad (5)$$

which is further equivalent to the following Linear programming problem

$$W_1(\mu, \nu) = \sup_{Af \leq c} m^T f, \quad (6)$$

with the following construction of matrix and vectors:

$$\begin{aligned}
m &:= (\mu(x_1), \dots, \mu(x_n), \nu(y_1), \dots, \nu(y_m))^T \in \mathbb{R}^{n+m}, \\
\phi &:= (f(x_1), \dots, f(x_n), -f(y_1), \dots, -f(y_m))^T \in \mathbb{R}^{n+m}, \\
c &:= (d(x_1, y_1), \dots, d(x_1, y_m), d(x_2, y_1), \dots, d(x_n, y_1), \dots, d(x_n, y_m), \\
&\quad d(y_1, x_1), \dots, d(y_m, x_1), d(y_1, x_2), \dots, d(y_1, x_n), \dots, d(y_m, x_n))^T \in \mathbb{R}^{nm}, \\
A &:= \begin{pmatrix} A_1 \\ A_2 \end{pmatrix}, \text{ where } A_1 := \begin{pmatrix} a_1 & I_m \\ a_2 & I_m \\ \vdots & \vdots \\ a_n & I_m \end{pmatrix}, A_2 := -A_1, a_i \in \mathbb{R}^{m \times n} \text{ with all ones at } i\text{-th column and zeros otherwise.}
\end{aligned}$$

A.2 Analytical and Algebraic Properties of Continuous Unified Ricci Curvature

To prove Proposition 3.8, we perceive edge weights $\omega \in \mathbb{R}^{n \times n}$ in its matrix form to keep in line with other linear algebra lemmas required in this section.

Lemma A.8. *s We say a matrix $A \in \mathbb{R}^{n \times n}$ is regular if for some $k \geq 1$, $A^k > 0$. Or equivalently, matrix A has non-negative entries and is strongly connected in our context. Then by Perron-Frobenius theorem:*

- There exists a unique positive unit left eigenvector \mathbf{v}_{pf} of A called Perron-Frobenius left eigenvector, whose corresponding eigenvalue λ_{pf} is real and has the largest norm among all eigenvalues.
- λ_{pf} is simple, i.e. has multiplicity one.

Proof. Perron-Frobenius theorem is well-known in the field of linear algebra, and has different forms on non-negative matrices, non-negative regular matrices and postivie matrices. We only need it for non-negative regular matrices. \square

Lemma A.9. *Let $A(t)$ be a differentiable matrix-valued function of t , $a(t)$ an eigenvalue of $A(t)$ of multiplicity one. Then we can choose an eigenvector $h(t)$ of $A(t)$ pertaining to the eigenvalue $a(t)$ to depend differentiably on t .*

Proof. For the purpose of our proof, we only need continuity of $h(t)$ on t , but we present this stronger statement, cf. Theorem 8, p130 in Lax [2007]. \square

Lemma A.10. *Suppose arbitrary matrix $B \in \mathbb{R}^{n \times n}$ is a non-negative regular matrix. Then its Perron-Frobenius left eigenvector \mathbf{v}_{pf} depend continuously on the B w.r.t. **small** perturbation ε entry-wise, restricting to B being non-negative and regular after the perturbation.*

Proof. Let E_{ij} denotes a matrix with zero entries except for entry (i, j) . Let $A(\varepsilon) := B + E_{ij}\varepsilon$, which is obviously a matrix-valued function differentiable w.r.t. ε . Suppose $|\varepsilon|$ is small such that we are only dealing with non-negative regular $A(\varepsilon)$. Therefore by Perron-Frobenius theorem A.8, there exists $\lambda_{pf}(\varepsilon)$ and $\mathbf{v}_{pf}(\varepsilon)$

for $A(\varepsilon)$, which has multiplicity 1. Therefore, by lemma A.9, we have that $\mathbf{v}_{pf}(\varepsilon)$ continuously depends on ε . Note that this eigenvector unnecessarily has unit length. But fortunately, the 2-norm of a positive continuous vector function is also continuous w.r.t. ε , we have that the Perron-measure $\mathbf{m} := \frac{\mathbf{v}_{pf}(\varepsilon)}{\|\mathbf{v}_{pf}(\varepsilon)\|}$ is continuous w.r.t. ε element-wise. \square

Lemma A.11. *The mean transition probability μ_x for vertex x defined in equation 5 is continuous w.r.t. weight matrix ω entry-wise, restricting to ω being non-negative and regular after the perturbation.*

Proof. By lemma A.10, we have that the Perron-measure \mathbf{m} is a continuous function w.r.t. ω entry-wise. Since $\forall x \in \mathcal{V}$, $\mathbf{m}(x) > 0$, we have $\forall x, y \in \mathcal{V}$, $\frac{\mathbf{m}(y)}{\mathbf{m}(x)}$ is continuous w.r.t. ω entry-wise.

Now we consider normalized weight W . WLOG, we suppose a perturbation of δ on ω in entry (i, j) , which only influences the i -th row of W . Denote this perturbed normalized weight matrix by W^* , and we have that

$$W^*(x, y) = \begin{cases} \frac{W(x, y)}{1+\delta} & \text{if } x = i, y \neq j \\ \frac{W(x, y) + \delta}{1+\delta} & \text{if } x = i, y = j \\ W(x, y) & \text{if } x \neq i \end{cases}$$

Therefore if we choose to perturb the (i, j) entry of W , the value of $W(x, y)$ is indifferent to this entry, hence continuous. For $W(i, y)$ where $y \neq j$, we pick $\varepsilon > 0$. By choosing $\delta \leq \frac{\varepsilon}{W(i, y) - \varepsilon}$, we ensure $W(x, y) - \frac{W(x, y)}{1+\varepsilon} \leq \varepsilon$, hence $W(i, y)$ is continuous w.r.t. ω entry-wise. For $W(i, j)$, we also pick $\varepsilon > 0$, and we choose $\delta \leq \frac{\varepsilon}{1 - W(i, j) - \varepsilon}$ to get the entry-wise continuity. Therefore, $\forall x \in \mathcal{V}$, the mean transition measure μ_x

$$\mu_x(y) := \frac{1}{2} \left[W(x, y) + \frac{\mathbf{m}(y)}{\mathbf{m}(x)} W(y, x) \right],$$

is a continuous function w.r.t. ω entry-wise, as summation and product of two continuous function is still continuous. \square

Lemma A.12. *Consider the convex optimization problem with a valid solution:*

$$\mathcal{M} := \inf_{Af \preceq c(t)} m^T f, \quad (7)$$

where $A \in \mathbb{R}^{n \times m}$, $f \in \mathbb{R}^{m \times 1}$, $m \in \mathbb{R}^{n \times 1}$, and $c(t): \mathbb{R} \mapsto \mathbb{R}^{n \times 1}$ being a vector-valued function that depends continuously on $t \in \mathbb{R}$. We claim that \mathcal{M} also depends continuously on t .

Proof. Note that equation 7 is a convex optimization problem and admits a feasible solution. Therefore the optimization problem admits strong duality from the Slater's condition and is equivalent to the following dual problem:

$$\begin{aligned} & \text{maximize} && -c(t)^T g \\ & \text{subject to} && A^T g + m = 0, \quad g \succeq 0. \end{aligned}$$

In particular, the maximization problem has \mathcal{M} as the optimal value. From the strong duality of convex optimization problem, we move the continuous function $c(t)$ from the constraint to the objective. Note that $-c(t)^T g$ is a continuous function of t , therefore the supremum over $-c(t)^T g$ is also a continuous function. \square

Lemma A.13. *Consider the convex optimization problem with a valid solution:*

$$\mathcal{M} := \inf_{Af \preceq c(t)} m(t)^T f,$$

where $A \in \mathbb{R}^{n \times m}$, $f \in \mathbb{R}^{m \times 1}$ and $m(t) : \mathbb{R} \mapsto \mathbb{R}^{n \times 1}$ and $c(t) : \mathbb{R} \mapsto \mathbb{R}^{n \times 1}$ being vector-valued functions that depend continuously on $t \in \mathbb{R}$. We claim that \mathcal{M} depends continuously on t .

Proof. We extend the lemma to the case where the objective is also a continuous function of t . Let $\delta > 0$ be a small perturbation, and $\mathcal{M}^* = \inf_{Af \preceq c(t+\delta)} m(t+\delta)^T f$. Therefore, we have that

$$\begin{aligned} |\mathcal{M} - \mathcal{M}^*| &= \left| \inf_{Af \preceq c} m^T f - \inf_{Af \preceq c^*} m^{*T} f \right| \\ &= \left| \inf_{Af \preceq c} m^T f - \inf_{Af \preceq c^*} m^T f + \inf_{Af \preceq c^*} m^T f - \inf_{Af \preceq c^*} m^{*T} f \right| \\ &\leq \left| \inf_{Af \preceq c} m^T f - \inf_{Af \preceq c^*} m^T f \right| + \left| \inf_{Af \preceq c^*} m^T f - \inf_{Af \preceq c^*} m^{*T} f \right| \end{aligned}$$

By lemma A.12 and continuity of supremum over continuous function, \mathcal{M} depends continuously on variable t . \square

The following is the proof of three important properties of CURC, the first one and the third one are natural results from the construction of κ_{CURC} , but we stress that the second note on continuity of κ_{CURC} is non-trivial and new.

Proposition A.14. *We have the following properties for κ_{CURC} :*

- (Unity) For connected unweighted-undirected graph $\mathcal{G} = (\mathcal{V}, \mathcal{E})$, for any pair of vertices $x, y \in \mathcal{V}$, we have $\kappa_{\text{CURC}}(x, y) = \kappa_{\text{OR}}(x, y)$.
- (Continuity) If we perceive $\kappa_{\text{CURC}}(x, y)$ as a function of ω , then $\kappa_{\text{CURC}}(x, y)$ is continuous w.r.t. ω entry-wise.
- (Scale Invariance) For strongly-connected weighted-directed graph $\mathcal{G} = (\mathcal{V}, \mathcal{E}, \omega)$, when all edge weights ω are scaled by an arbitrary positive constant λ , the value of $\kappa_{\text{CURC}}(x, y)$ for any $x, y \in \mathcal{V}$ is unchanged.

Proof. We prove the properties by sequential order.

1. Proof of Unity

Suppose A to be the adjacency matrix (binary) of unweighted-undirected graph $\mathcal{G} = (\mathcal{V}, \mathcal{E})$ and we are interested in κ_{CURC} for $x, y \in \mathcal{V}$. Let $\mathcal{M} :=$ the length of the longest shortest path. Intuitively, by the definition of the

ε -masked CURC in Definition 3.7, we may pick ε sufficiently small, such that none of the “virtual edges” are masked, as edge length $\frac{1}{\varepsilon}$ will not be picked in calculating the weighted shortest distance. By picking $\varepsilon < \frac{1}{\mathcal{M}}$, the “virtual edges” have length even more than the longest distance in \mathcal{G} , resulting $\forall x, y \in \mathcal{V}$, $d(x, y)$ is independent of these “virtual edges”. When \mathcal{G} is unweighted-undirected, the adjacency matrix A is symmetric. Therefore the Perron-measure $\mathbf{m}(x)$ for each vertex x is proportional to the inverse degree $\frac{1}{d_x}$. By direct calculation, we have $W(x, y) = \frac{1}{d_x}$ and $W(y, x) = \frac{1}{d_y}$. Therefore, the mean transition distribution

$$\mu_x(y) = \frac{1}{2} \left[\frac{1}{d_x} + \frac{d_y}{d_x \times d_y} \right] = \frac{1}{d_x},$$

which is equivalent to the initial mass placement in the construction of Ollivier-Ricci Curvature κ_{OR} .

Since the initial mass distribution according for κ_{CURC} and κ_{OR} is the same and we choose ε sufficiently small, namely when $\varepsilon < \frac{1}{\mathcal{M}}$, the masked and unmasked Wasserstein distances are equal: $\mathcal{W}_1^\varepsilon(\mu_x, \mu_y) = \mathcal{W}_1(\mu_x, \mu_y)$. It is straightforward that the shortest weighted distance d is positively related to ε . Hence $\kappa_{CURC}^\varepsilon$ is a decreasing function in ε . But for a fixed graph \mathcal{G} , $\kappa_{CURC}^\varepsilon$ is invariant when $\varepsilon < \frac{1}{\mathcal{M}}$. Therefore the limit of $\kappa_{CURC}^\varepsilon$ indeed tends to κ_{OR} as $\varepsilon \rightarrow 0$. Therefore, $\kappa_{CURC} = \kappa_{OR}$ on connected unweighted-undirected graphs.

2. Proof of Continuity

To prove the entry-wise continuity of CURC w.r.t. weight matrix ω under the assumption that perturbation ensures ω to be non-negative and regular, we use the supremum form of Wasserstein distance from the Kantorovich–Rubinstein duality:

$$\mathcal{W}_1^\varepsilon(\mu_x, \mu_y) = \sup_{f \in \text{Lip}(1)} \sum_{z \in \mathcal{V}} f(z) (\mu_y(z) - \mu_x(z)), \quad (8)$$

where $\forall x, y \in V$, $f(y) - f(x) \leq d^\varepsilon(x, y)$ as $f \in \text{Lip}(1)$. We may exploit the limit definition of $\mathcal{W}_1^\varepsilon$ and take ε sufficiently small so that d^ε and $\mathcal{W}_1^\varepsilon$ is independent of ε , hence we may abuse the notation, denote $d^\varepsilon(x, y)$ as $d(x, y)$ and $\mathcal{W}_1^\varepsilon(\mu_x, \mu_y)$ as $\mathcal{W}_1(\mu_x, \mu_y)$ for $x, y \in \mathcal{V}$. We first show that $\forall x \neq y \in \mathcal{V}$, $d(x, y)$ is continuous entry-wise w.r.t. ω . Let \mathcal{M} be the diameter w.r.t. edge length as inverse edge weights $\frac{1}{\omega}$, and for edge with 0 weight we treat the edge length as $+\infty$. Suppose there is a small perturbation of δ on an arbitrary entry of ω after which the weight matrix is still non-negative regular, we denote the new weight matrix as ω^δ and distance function as d^δ on this perturbed matrix. WLOG, we assume the perturbation is smaller than the smallest positive entry and we let ω^{\min} to be this minimal positive entry of ω . With this small perturbation, we have

$$|d(x, y) - d^\delta(x, y)| \leq \frac{1}{\omega^{\min} - \delta} - \frac{1}{\omega^{\min}}.$$

Therefore, $\forall \varepsilon_0$, let $\delta \leq \frac{\omega^2 \varepsilon_0}{1 + \omega \varepsilon_0}$, we have $|d(x, y) - d^\delta(x, y)| \leq \varepsilon_0$, hence $d(x, y)$ is continuous entry-wise w.r.t. ω .

We will prove the continuity of

$$\frac{\mathcal{W}_1(\mu_x, \mu_y)}{d(x, y)} = \sup_{f \in \text{Lip}(1)} \sum_{z \in \mathcal{V}} f(z) \frac{\mu_y(z) - \mu_x(z)}{d(x, y)},$$

which is sufficient for the overall continuity of CURC. By corollary A.7, we have that

$$\mathcal{W}_1(\mu_x, \mu_y) = \sup_{Af \preceq c} m^T f.$$

By previous argument, m as a function of mean transition measure μ and c as a function of distance function d are both continuous w.r.t. ω entry-wise. Therefore, $\mathcal{W}_1(\mu_x, \mu_y)$ is indeed a continuous function w.r.t. ω entry-wise by lemma A.13. Since $d(x, y)$ is positive and continuous entry-wise, we conclude that κ_{CURC} is continuous entry-wise w.r.t. ω .

3. Proof of Scale Invariance

The third property is straightforward from the construction of the **reciprocal edge weight** \mathbf{r}^ε in Definition 3.5. Suppose $\mathcal{G}(\mathcal{V}, \mathcal{E}, \omega)$ to be the unscaled strongly-connected weighted-directed graph and $\mathcal{G}^*(\mathcal{V}, \mathcal{E}, \omega^*)$ be the scaled one, where $\omega^* = \lambda \omega$. Let \mathcal{M} and \mathcal{M}^* be the diameter of \mathcal{G} and \mathcal{G}^* respectively w.r.t. the **reciprocal edge weight**. Note we are not considering the ε -masked edge weight for computing the diameter, in the sense that for non-existent edges, the edge length is $+\infty$. \mathcal{M} and \mathcal{M}^* are well-defined due to strongly-connectivity.

After a scale wof λ , the eigenvalues of ω and ω^* differ by a factor of λ . By Perron-Frobenius theorem, the corresponding Perron-measure \mathbf{m} and \mathbf{m}^* are the same. Similarly, it is straightforward that the random walk matrices W and W^* are also the same. Therefore the initial measure μ of \mathcal{G} coincides with μ^* of \mathcal{G}^* .

Since $\lambda > 0$, we can find ε small enough, so that $\frac{1}{\varepsilon} > \max\{\mathcal{M}, \mathcal{M}^*\}$, ensuring the distance function d^ε and $d^{\varepsilon*}$ are independent of ε . Hence, for this choice of ε , $\forall x \neq y \in \mathcal{V}$, $d^{\varepsilon*}(x, y) = \lambda d^\varepsilon(x, y)$. By Kantorovich–Rubinstein duality 3.4, we have that

$$\begin{aligned} \mathcal{W}_1^{\varepsilon*}(x, y) &= \inf_{\pi \in \Pi(\mu_x, \mu_y)} \sum_{x, y \in \mathcal{V}} d^*(x, y) \pi(x, y) \\ &= \inf_{\pi \in \Pi(\mu_x, \mu_y)} \sum_{x, y \in \mathcal{V}} \lambda d(x, y) \pi(x, y) \\ &= \lambda \mathcal{W}_1^\varepsilon(x, y). \end{aligned}$$

Therefore,

$$\begin{aligned}
\kappa_{CURC}^* &= \lim_{\varepsilon \rightarrow 0} \kappa_{CURC}^{\varepsilon*}(x, y) \\
&= \lim_{\varepsilon \rightarrow 0} \left(1 - \frac{\mathcal{W}_1^{\varepsilon*}(\mu_x, \mu_y)}{d^{\varepsilon*}(x, y)}\right) \\
&= \lim_{\varepsilon \rightarrow 0} \left(1 - \frac{\lambda \mathcal{W}_1^\varepsilon(\mu_x, \mu_y)}{\lambda d^\varepsilon(x, y)}\right) \\
&= \lim_{\varepsilon \rightarrow 0} \left(1 - \frac{\mathcal{W}_1^\varepsilon(\mu_x, \mu_y)}{d^\varepsilon(x, y)}\right) \\
&= \kappa_{CURC},
\end{aligned}$$

as required. Therefore, CURC is scale invariant. □

A.3 Continuous Unified Ricci Curvature and Bottlenecking

To reveal the geometric connection between Continuous Unified Ricci Curvature and propagation graphs, we introduce the concept of *Dirichlet isoperimetric constant* \mathcal{I}_V^D , which is the extension of the well-known cheeger constant into strongly-connected weighted-directed graphs. We perceive \mathcal{I}_V^D as a measure of bottlenecking on weighted graphs and state that when CURC has a lower bound K , \mathcal{I}_V^D has a lower bound that is positively related to K . Our proof draws its foundation from the derivation presented in [Ozawa et al. \[2020\]](#), where they prove the result on strongly-connected weighted-directed graph with unit edge length. Few minor modifications are required to adapt the result to our scenario concerning weighted edge lengths. We will identify and elucidate the key elements that require clarification, while also presenting the results that remain unchanged.

Definition A.15. (Chung Laplacian) Let $\mathcal{G} = (\mathcal{V}, \mathcal{E}, \omega)$ be a finite strongly-connected weighted directed-graph and $f : \mathcal{V} \mapsto \mathbb{R}$. Suppose $\mu : \mathcal{V} \times \mathcal{V} \mapsto [0, 1]$ is a probability kernel satisfying $\sum_{y \in \mathcal{V}} \mu(x, y) = 1$ for all $x \in \mathcal{V}$. The *Chung Laplacian* \mathcal{L} on function f associated with μ is defined as

$$\mathcal{L}f(x) := f(x) - \sum_{y \in \mathcal{V}} \mu(x, y)f(y).$$

Let $d : \mathcal{V} \times \mathcal{V} \mapsto \mathbb{R}^{\geq 0}$ be a distance function (asymmetric). For each vertex $x \in \mathcal{V}$, the *asymptotic mean curvature* \mathcal{H}_x is defined by

$$\mathcal{H}_x := \mathcal{L}\rho_x(x),$$

where $\rho_x : \mathcal{V} \rightarrow \mathbb{R}$ is the distance from x defined as $\rho_x(y) := d(x, y)$. Note that with weighted shortest distance d , $\mathcal{H}_x \in (-\infty, 0)$.

For each vertex $x \in \mathcal{V}$, the $\text{InRad}_x \mathcal{V}$ of \mathcal{V} at vertex x is defined by

$$\text{InRad}_x \mathcal{V} := \sup_{y \in \mathcal{V}} \rho_x(y),$$

And for any $x \in \mathcal{V}$ and $R > 0$, we set $E_R(x) := \{y \in V \mid \rho_x(y) \geq R\}$.

Definition A.16. (Boundary Perron-measure) For a non-empty $\Omega \subset \mathcal{V}$, its *Boundary Perron-measure* is defined as

$$\mathbf{m}(\partial\Omega) := \sum_{y \in \Omega} \sum_{z \in V \setminus \Omega} \mathbf{m}_{yz},$$

where $\mathbf{m}_{yz} := \mathbf{m}(y)\mu(y, z)$ and $\mathbf{m}(\Omega) = \sum_{x \in \Omega} \mathbf{m}(x)$.

Definition A.17. (Dirichlet isoperimetric constant) The *Dirichlet isoperimetric constant* $\mathcal{I}_{\mathcal{V}}^D$ on \mathcal{V} is defined by

$$\mathcal{I}_{\mathcal{V}}^D := \inf_{\Omega} \frac{\mathbf{m}(\partial\Omega)}{\mathbf{m}(\Omega)},$$

which is analogous to cheeger constant on weighted-directed graph.

Exploiting definition 3.7 on Continuous Unified Ricci Curvature, we introduce a limit version of **CURC** concerning idleness for theoretical derivation.

Definition A.18. (α -idle Mean Transition probability Kernel) Define the *α -idle Mean Transition probability Kernel* by

$$\mu_x^\alpha(y) = \mu^\alpha(x, y) := \begin{cases} \frac{1}{2}\alpha[W(x, y) + \frac{\mathbf{m}(y)}{\mathbf{m}(x)}W(y, x)] & \text{if } y \neq x \\ (1 - \alpha) & \text{if } y = x \end{cases} \quad (9)$$

In the following, we use the same ε -masked reciprocal weighted edge length for calculating Wasserstein distance.

Definition A.19. (Idle-CURC) Define the *α -idle ε -masked Continuous Unified Ricci Curvature* and *α -idle Continuous Unified Ricci Curvature* by

$$\begin{aligned} \kappa_{\text{CURC}}^{\varepsilon\alpha}(x, y) &:= 1 - \frac{\mathcal{W}_1^\varepsilon(\mu_x^\alpha, \mu_y^\alpha)}{d^\varepsilon(x, y)}, \\ \kappa_{\text{CURC}}^\alpha(x, y) &:= \lim_{\varepsilon \rightarrow 0} \frac{\kappa_{\text{CURC}}^{\varepsilon\alpha}(x, y)}{\alpha} \end{aligned}$$

The *idle-CURC* is defined by

$$\kappa_{\text{CURC}}^I(x, y) := \lim_{\varepsilon \rightarrow 0} \lim_{\alpha \rightarrow 0} \frac{\kappa_{\text{CURC}}^{\varepsilon\alpha}(x, y)}{\alpha}.$$

Theorem A.20. Let $\mathcal{G} = (\mathcal{V}, \mathcal{E}, \omega)$ be a strongly-connected weighted-directed graph, we have that for all $x \neq y \in \mathcal{V}$,

$$\kappa_{\text{CURC}}^I(x, y) \geq \kappa_{\text{CURC}}(x, y).$$

Proof. Using the trick mentioned in the proof of A.14, we choose ε sufficiently small such that $\kappa_{\text{CURC}}^{\varepsilon\alpha}(x, y)$ is independent of ε . WLOG, we abbreviate $\kappa_{\text{CURC}}^{\varepsilon\alpha}(x, y)$ as $\kappa_{\text{CURC}}^{\alpha}(x, y)$. By lemma 3.2 from Ozawa et al. [2020], $\kappa_{\text{CURC}}^{\alpha}(x, y)$ is concave in $\alpha \in [0, 1]$ and $\frac{\kappa_{\text{CURC}}^{\alpha}(x, y)}{\alpha}$ is non-increasing in $\alpha \in (0, 1]$. Note that $\kappa_{\text{CURC}}(x, y)$ is nothing but $\frac{\kappa_{\text{CURC}}^{\alpha}(x, y)}{\alpha}$ taking $\alpha = 1$. Therefore by monotonicity, $\kappa_{\text{CURC}}^I(x, y) \geq \kappa_{\text{CURC}}(x, y)$. \square

Proposition A.21. *Let $\Omega \subset \mathcal{V}$ be a non-empty subset. Then for all function $f_0, f_1 : \mathcal{V} \rightarrow \mathbb{R}$,*

$$\begin{aligned} \sum_{x \in \Omega} \mathcal{L}f_0(x)f_1(x)\mathbf{m}(x) &= \frac{1}{2} \sum_{x, y \in \Omega} (f_0(y) - f_0(x))(f_1(y) - f_1(x)) \mathbf{m}_{xy} \\ &\quad - \sum_{x \in \Omega} \sum_{y \in V \setminus \Omega} (f_0(y) - f_0(x)) f_1(x) \mathbf{m}_{xy}. \end{aligned}$$

Proof. The proof is a merely a calculation similar to integration by part. We stress that the result only depends on fact that \updownarrow is symmetric. (c.f. Theorem 2.1 in Grigor'yan [2018]) \square

Lemma A.22. *Let $x, y \in \mathcal{V}$ with $x \neq y$. Then*

$$\kappa_{\text{CURC}}^{\alpha}(x, y) = \inf_{f \in \text{Lip}_1(\mathcal{V})} \left(\frac{1}{\alpha} (1 - \nabla_{xy}f) + \nabla_{xy}\mathcal{L}f \right),$$

where $\nabla_{xy}f := \frac{f(y) - f(x)}{d(x, y)}$.

Proof. We refer to lemma 3.9 in Ozawa et al. [2020], which is essentially similar. It is worth noticing that we are using a different weighted distance function, but there is no restriction on the distance function in the proof. \square

Proposition A.23. *Let $x, y \in \mathcal{V}$ with $x \neq y$. Suppose $\mathcal{F}_{xy} := \{f \in \text{Lip}_1(\mathcal{V}) \mid \nabla_{xy}f = 1\}$. Then we have*

$$\kappa_{\text{CURC}}^I(x, y) = \inf_{f \in \mathcal{F}_{xy}} \nabla_{xy}\mathcal{L}f.$$

Proof. We refer to theorem 3.10 in Ozawa et al. [2020], where the only part worth mentioning is that we require

$$\text{Lip}_{1,x}(V) := \{f \in \text{Lip}_1(V) \mid f(x) = 0\},$$

to be compact w.r.t. the canonical topology on \mathbb{R}^n . Let $\omega^* := \inf_{x, y \in \mathcal{V}} \omega(x, y) > 0$, then $d(x, y) \leq \frac{n}{\omega^*}$, which is bounded for fixed weight matrix ω . As we restrict $f(x) = 0$, the 1-Lipshitz function f w.r.t. the weighted shortest distance function d is still bounded. Therefore, changing the distance function does not break compactness w.r.t. \mathbb{R}^n . \square

Theorem A.24. *Let $x \in V$. For $K \in \mathbb{R}$ we assume $\inf_{y \in V \setminus \{x\}} \kappa_{\text{CURC}}^I(x, y) \geq K$. For $\Lambda \in (-\infty, 0)$ we further assume $\mathcal{H}_x \geq \Lambda$. Then on $V \setminus \{x\}$, we have*

$$\mathcal{L}\rho_x \geq K\rho_x + \Lambda$$

Proof. Fix a vertex $x \in \mathcal{V}$. Note that the distance function $\rho_x \in \mathcal{F}_{xy}$ defined in proposition A.23, as $\nabla_{xy}\rho_x = \frac{\rho_x(y) - \rho_x(x)}{d(x,y)} = 1$. Hence, for all $y \in \mathcal{V} \setminus \{x\}$,

$$K \leq \kappa_{CURC}^I(x, y) \leq \nabla_{xy}\mathcal{L}\rho_x = \frac{\mathcal{L}\rho_x(y) - \mathcal{L}\rho_x(x)}{d(x, y)} \leq \frac{\mathcal{L}\rho_x(y) - \Lambda}{d(x, y)}.$$

When $y = x$, the result is direct from $\mathcal{H}_x \geq \Lambda$. Hence, $\mathcal{L}\rho_x \geq KR + \Lambda$. \square

Theorem A.25. *Let $x \in V$. For $K \in \mathbb{R}$ we assume $\inf_{y \in V \setminus \{x\}} \kappa_{CURC}(x, y) \geq K$. For $\Lambda \in (-\infty, 0)$ we also assume $\mathcal{H}_x \geq \Lambda$. For $D > 0$ we further assume $\text{InRad}_x V \leq D$. Then for every $R > 0$ with $KR + \Lambda > 0$, we have*

$$\mathcal{I}_{E_R(x)}^D \geq \frac{KR + \Lambda}{D}$$

Proof. The proof is analogue to Proposition 9.6 in Ozawa et al. [2020], while we include the proof utilizing previous results for completeness. By theorem A.20, $\kappa_{CURC}(x, y) \geq K$ implies $\kappa_{CURC}^I(x, y) \geq K$. Let $\Omega \subset E_R(x)$ be a non-empty vertex set. By Proposition A.21, we have

$$\begin{aligned} - \sum_{y \in \Omega} \mathcal{L}\rho_x(y)\mathbf{m}(y) &= \sum_{y \in \Omega} \sum_{z \in V \setminus \Omega} (\rho_x(z) - \rho_x(y)) \mathbf{m}_{yz} \\ &\geq - \sum_{y \in \Omega} \sum_{z \in V \setminus \Omega} \rho_x(y) \mathbf{m}_{yz} \\ &\geq -D\mathbf{m}(\partial\Omega) \end{aligned}$$

By theorem A.24, for all $y \in \Omega$,

$$\mathcal{L}\rho_x(y) \geq KR + \Lambda$$

Therefore,

$$\begin{aligned} \sum_{y \in \Omega} [\mathcal{L}\rho_x(y) - (KR + \Lambda)]\mathbf{m}(y) &\geq 0 \\ \Rightarrow \sum_{y \in \Omega} \mathcal{L}\rho_x(y)\mathbf{m}(y) &\geq \sum_{y \in \Omega} KR\mathbf{m}(y) = (KR + \Lambda)\mathbf{m}(\Omega). \end{aligned}$$

Note that we have $\sum_{y \in \Omega} \mathcal{L}\rho_x(y)\mathbf{m}(y) \leq D\mathbf{m}(\partial\Omega)$, which combined together yields

$$\begin{aligned} D\mathbf{m}(\partial\Omega) &\geq (KR + \Lambda)\mathbf{m}(\Omega) \\ \Rightarrow \frac{\mathbf{m}(\partial\Omega)}{\mathbf{m}(\Omega)} &\geq \frac{(KR + \Lambda)}{D} \\ \Rightarrow \mathcal{I}_{E_R(x)}^D &\geq \frac{KR + \Lambda}{D} \end{aligned}$$

\square

Before we end the discussion of properties of Continuous Unified Ricci Curvature, we point out that computing optimal-transportation based graph curvature can be computational intensive from solving a Linear programming problem similar to corollary A.7. In Topping et al. [2022] they provide a lower bound estimation for the Ollivier-ricci graph curvature. Likewise, we provide a universal lower bound for CURC using Kantorovich-Rubinstein duality and a tighter lower bound for CURC under stronger assumptions.

Proposition A.26. *Based on the construction of CURC, we choose ε sufficiently small s.t. distance function d^ε is independent of ε and denote it as d . Let $\mathcal{D}(x, y) := \max\{d(x, y), d(y, x)\}$ be the largest weighted distance between vertices x and y . For distinct vertices $x, y \in \mathcal{V}$, we have*

$$\begin{aligned} \kappa_{\text{CURC}}(x, y) \geq & -\frac{2\mathcal{D}(x, y)}{d(x, y)}(1 - \mu(x, y) - \mu(y, x))_+ + \frac{1}{d(x, y)}(d(x, y) + \mathcal{D}(x, y) - \mathcal{H}(y, x)) \\ & - \frac{\mathcal{D}(x, y) - d(y, x)}{d(x, y)}(\mu(x, y) + \mu(y, x)), \end{aligned}$$

where $\mathcal{H}(x, y)$ is defined by

$$\begin{aligned} \tilde{\mathcal{H}}(x) &:= -\sum_{y \in \mathcal{V}} \mu(x, y)d(y, x) \\ \mathcal{H}(x) &:= -\sum_{y \in \mathcal{V}} \mu(x, y)d(x, y) \\ \mathcal{H}(x, y) &:= -\sum_{y \in \mathcal{V}} \mu(x, y)d(x, y) - \sum_{y \in \mathcal{V}} \mu(x, y)d(y, x) = \tilde{\mathcal{H}}(x) + \mathcal{H}(x). \end{aligned}$$

Proof. The proof is a simple calculation of the Kantorovich-Rubinstein duality and we present the proof along the line of Proposition 6.1 in Ozawa et al. [2020]. By theorem 3.4, we have

$$\begin{aligned} \mathcal{W}_1(\mu_x, \mu_y) &= \sup_{f \in \text{Lip}(1)} \sum_{z \in \mathcal{V}} f(x)(\mu_x(z) - \mu_y(z)) \\ &= \sup_{f \in \text{Lip}(1)} \left\{ \left(\sum_{z \in \mathcal{V} \setminus \{x\}} (f(z) - f(y))\mu(y, z) \right) - \left(\sum_{z \in \mathcal{V} \setminus \{y\}} (f(z) - f(x))\mu(x, z) \right) \right. \\ &\quad \left. + (f(y) - f(x))(1 - \mu(x, y) - \mu(y, x)) \right\}. \end{aligned}$$

For an arbitrary function $f \in \text{Lip}(1)$ w.r.t. d , we have that

$$f(z) - f(y) \leq d(y, z), \quad f(z) - f(x) \geq -d(z, x), \quad |f(y) - f(x)| \leq \mathcal{D}(x, y),$$

Therefore,

$$\begin{aligned}
\mathcal{W}_1(\mu_x, \mu_y) &\leq \sum_{z \in V \setminus \{x\}} d(y, z) \mu(y, z) + \sum_{z \in V \setminus \{y\}} d(z, x) \mu(x, z) \\
&\quad + \mathcal{D}(x, y) |1 - \mu(x, y) - \mu(y, x)| \\
&= (-\mathcal{H}_y - d(y, x) \mu(y, x)) + \left(-\overleftarrow{\mathcal{H}}_x - d(y, x) \mu(x, y) \right) \\
&\quad + \mathcal{D}(x, y) (2(1 - \mu(x, y) - \mu(y, x))_+ - (1 - \mu(x, y) - \mu(y, x))) \\
&= \mathcal{H}(y, x) - d(y, x) (\mu(x, y) + \mu(y, x)) \\
&\quad + \mathcal{D}(x, y) (2(1 - \mu(x, y) - \mu(y, x))_+ - (1 - \mu(x, y) - \mu(y, x))) \\
&= 2\mathcal{D}(x, y) (1 - \mu(x, y) - \mu(y, x))_+ - (\mathcal{D}(x, y) - \mathcal{H}(y, x)) \\
&\quad + (\mathcal{D}(x, y) - d(y, x)) (\mu(x, y) + \mu(y, x)).
\end{aligned}$$

Hence,

$$\begin{aligned}
\kappa_{CURC}(x, y) &= 1 - \frac{\mathcal{W}_1(\mu_x, \mu_y)}{d(x, y)} \\
&\geq 1 - 2 \frac{\mathcal{D}(x, y)}{d(x, y)} (1 - \mu(x, y) - \mu(y, x))_+ - \frac{1}{d(x, y)} (\mathcal{D}(x, y) - \mathcal{H}(y, x)) \\
&\quad + \frac{(\mathcal{D}(x, y) - d(y, x))}{d(x, y)} (\mu(x, y) + \mu(y, x)) \\
&= -\frac{2\mathcal{D}(x, y)}{d(x, y)} (1 - \mu(x, y) - \mu(y, x))_+ + \frac{1}{d(x, y)} (d(x, y) + \mathcal{D}(x, y) - \mathcal{H}(y, x)) \\
&\quad - \frac{\mathcal{D}(x, y) - d(y, x)}{d(x, y)} (\mu(x, y) + \mu(y, x)).
\end{aligned}$$

□

Remark A.27. To calculate this lower bound, after pre-processing distance function d and the mean transition probability, the asymptotic complexity is $\mathcal{O}(n)$ for each vertex pair $x \neq y$. The pre-processing includes a Floyd-Washall algorithm for shortest path which is $\mathcal{O}(n^3)$ and a power method for computing perron eigenvectors which is conventionally $\mathcal{O}(n^2)$. Therefore, the overall computational complexity is $\mathcal{O}(n^3)$.

When strongly-connected $\mathcal{G} = (\mathcal{V}, \mathcal{E}, \omega)$ satisfies $(x, y) \in \mathcal{E} \iff (y, x) \in \mathcal{E}$, and we use edge length 1 for computing the shortest distance, CURC degenerates to the curvature definition in Ozawa et al. [2020]. Under this stronger assumption, we can achieve a tighter bound for κ_{CURC} with a specific transportation plan utilizing the topology of local neighborhoods.

Definition A.28. For $x \sim y$, we define

- $\vec{\mathcal{N}}_x := \{y \in V \mid x \rightarrow y\}$, $\overleftarrow{\mathcal{N}}_x := \{y \in V \mid y \rightarrow x\}$, $\mathcal{N}_x := \vec{\mathcal{N}}_x \cup \overleftarrow{\mathcal{N}}_x$, which are *inner neighborhood*, *outer neighborhood* and *neighborhood* respectively. If $\forall x, y \in \mathcal{V}$, $x \rightarrow y$ implies $y \rightarrow x$, then $\vec{\mathcal{N}}_x = \overleftarrow{\mathcal{N}}_x = \mathcal{N}_x$. Hence we use notation \mathcal{N}_x to denote neighborhood for x .

- $\Delta(x, y) := \mathcal{N}_x \cap \mathcal{N}_y$ denotes set of common neighbors of vertices x and y .
- $\square(x, y) := \{z \in \mathcal{N}_x \setminus \mathcal{N}_y, z \neq y : \exists w \in (\mathcal{N}_z \cap \mathcal{N}_y) \setminus \mathcal{N}_x\}$, which denotes the neighbors of x forming 4-cycle based at $x \sim y$ without diagonals inside.
- $\square^m(x, y) := \max\{|U| : U \subseteq \square(x, y), \exists \varphi : U \rightarrow \square(y, x), \varphi \in \mathcal{D}(U)\}$, and we use φ^m to denote one such optimal pairing between $\square(x, y)$ and $\square(y, x)$.

Proposition A.29. *On a strongly-connected weighted-directed locally graph $G=(\mathcal{V}, \mathcal{E}, \omega)$, where $\forall x, y \in \mathcal{V}$, if $x \rightarrow y \iff y \rightarrow x$, we have that if $x \sim y$, then*

$$\begin{aligned} \kappa_{CURC}(x, y) \geq & - \left(1 - \mu(x, y) - \mu(y, x) - \sum_{z \in \Delta(x, y)} \mu(x, z) \vee \mu(y, z) - \sum_{z \in \square(x, y)} \mu(x, z) \wedge \mu(y, \varphi^m(z)) \right)_+ \\ & - \left(1 - \mu(x, y) - \mu(y, x) - \sum_{z \in \Delta(x, y)} \mu(x, z) \wedge \mu(y, z) - \sum_{z \in \square(x, y)} \mu(x, z) \wedge \mu(y, \varphi^m(z)) \right)_+ \\ & + \sum_{z \in \Delta(x, y)} \mu(x, z) \wedge \mu(y, z). \end{aligned}$$

Remark A.30. When $\mathcal{G} = (\mathcal{V}, \mathcal{E}, \omega)$ satisfies $x \rightarrow y \iff y \rightarrow x$, optimal transportation based curvature of $x \sim y$ is only dependent up to cycles of size at most 5. In theorem 6 of [Jost and Liu \[2014\]](#), they give a bound concerning the influence of triangles and in theorem 2 of [Topping et al. \[2022\]](#), they extend the result concerning cycles of size 4. The proof of this lower bound is in line with these two theorems and we give a tighter lower bound for κ_{CURC} concerning the influence of 4-cycles compared to proposition A.26 under this stronger assumption. The computational cost for computing this lower bound is at most $\mathcal{O}(n^4)$. We stress that under specific user case for CURC which requires lower computational cost, the lower bound estimations for κ_{CURC} from proposition A.26 and proposition A.29 become handy.

B Expressiveness of GPNNs

B.1 Color refinement(CR)

The 1-dimensional Weisfeiler-Lehman algorithm (1-WL), also referred to as the color-refinement algorithm, operates iteratively to determine a color mapping $\mathcal{X}_{\mathcal{G}} : \mathcal{V} \mapsto \mathcal{C}$ for a given graph $\mathcal{G} = (\mathcal{V}, \mathcal{E})$, where \mathcal{C} represents the set of colors. Every vertex is initially assigned an identical color. During each ensuing iteration, a hash function is utilized by the 1-WL algorithm to amalgamate the current color of each vertex with the colors of its adjacent vertices, thereby updating the vertex’s color. The algorithm persists in this process for a substantial number of iterations T , typically set to $T = |\mathcal{V}|$.

B.2 Prototypical GPNNs

It is well known that most of the MPNNs have an expressiveness upper bound of 1-WL [Xu et al., 2019, Morris et al., 2019a]. For GPNNs, the situation is a bit different due to the fact that we have the propagation depends on adjacency function $F(\mathbf{A})$, which is any permutation equivariant function.

Here we set two prototypical GPNNs to analyze their expressiveness. First, we consider the GPNNs with homogeneous adjacency features across all heads and layers and refer to them as **Static GPNNs**.

$$F = F^l \tag{10}$$

For generality, we also consider the case when multiple adjacency function F is used in the model. An extra prototype model is defined with recurrence as a special case of **Dynamic GPNNs**

$$F^l = F^{l+p} \tag{11}$$

In order to reach the upper-bounded expressiveness, the model would be assumed to have a sufficient number of heads and two MLPs with a sufficient layer and width for the connectivity function and update function.

Lemma B.1. [Xu et al., 2019], **Lemma 5** *If we assume that the set \mathcal{X} is countable, a function $f : \mathcal{X} \mapsto \mathbb{R}^n$ can be established such that each bounded-size multiset $\hat{\mathcal{X}} \subset \mathcal{X}$ has a unique corresponding function $h(\hat{\mathcal{X}}) := \sum_{x \in \hat{\mathcal{X}}} f(x)$. Additionally, a decomposition of any multiset function g can be represented as $g(\hat{\mathcal{X}}) = \phi(\sum_{x \in \hat{\mathcal{X}}} f(x))$ for some function ϕ .*

Proposition B.2. (Static GPNNs) *Suppose GPNN model M has a fixed adjacency feature $[f_{uv}]_{u,v \in \mathcal{V}}$, with sufficient heads and layers, the expressiveness of M is upper-bounded by the iterative color-refinement*

$$\mathcal{X}_{\mathcal{G}}^{t+1}(v) = \text{hash}\{(\mathcal{X}_{\mathcal{G}}^t(u), f_{vu}) : u \in \mathcal{V}\} \tag{12}$$

Proof. First, we prove that for any f_{uv} there exists a function π_{base} which is injective from each entry of $f_{uv} = [F(A)]_{uv}$, to \mathbb{R} . Here we define the set of all possible values of

$$F_n := \{[F(A)]_{uv} : A = \text{adj}(\mathcal{G}), \mathcal{G} = (\mathcal{V}, \mathcal{E}), |\mathcal{V}| \leq n, (v, u) \in \mathcal{V}^2\} \quad (13)$$

For all graphs with no more than n nodes, the total number of possible values of $f_{vu} \in \mathbb{R}^d$ is finite and depends on n and F , denoted as $|F_n| = N$. Given arbitrary bijection $\text{id} : F_n \mapsto [N]$, By the Stone–Weierstrass Theorem applied to the algebra of continuous functions $C(\mathbb{R}^d, \mathbb{R})$ there exists a polynomial π_{base} so that

$$\pi_{base}(f) = \text{id}(f), \text{ for any } f \in F_n \quad (14)$$

Now, we are ready to construct the π^h using π_{base} combined with the indicator function $\pi_1^h(d) := \mathbb{I}(d = h)$. For each head, we have $\pi^h = \pi_1^h \circ \pi_{base}$. By multiplying \mathbf{P} with $\phi(\mathbf{X})$, we can recover the color-refinement of

$$\begin{aligned} \chi_{\mathcal{G}}^l(v) &:= \text{hash} \left(\left(\chi_{\mathcal{G}}^{l,1}(v), \chi_{\mathcal{G}}^{l,2}(v), \dots, \chi_{\mathcal{G}}^{l,|F_n|}(v) \right) \right), \\ \text{where } \chi_{\mathcal{G}}^{l,h}(v) &:= \{ \{ \chi_{\mathcal{G}}^{l-1}(u) : u \in \mathcal{V}, \text{id}(f_{vu}) = h \} \}. \end{aligned} \quad (15)$$

In detail: by applying **Lemma B.1** to matrix multiplication, we fulfill the injective multiset function in 15.

$$\mathbf{X}_v^{l,h} = \sum_{u \in \{\pi^h(f(A)_{v,u})=1\}} \phi(\mathbf{X}_u^l) \quad (16)$$

By concatenating all the heads (injective) and passing them to an **MLP** update function, we can fulfill the hash function in 15. Before conclusion, we refer to the universal approximation theorem of **MLPs** [Hornik et al., 1989] to validate the use of **MLPs** to approximate constructed functions. Finally, it’s easy to see that the color refinement in 15 is identical to 12 \square

Proposition B.3. (Dynamic GPNNs) *Suppose GPNN model M has a layer-dependent propagation function $F^l(\mathbf{A})$, repeats every p layer: $F^l = F^{l+p}$. With sufficient heads and layers, by stacking repetitions of such repetition, the expressiveness of M is upper-bounded by the iterative color refinement*

$$\mathcal{X}_{\mathcal{G}}^{t+1}(v) = \text{hash} \{ \{ (\mathcal{X}_{\mathcal{G}}^t(u), (f_{vu}^1, f_{vu}^2, \dots, f_{vu}^p)) : u \in \mathcal{V} \} \} \quad (17)$$

In order to prove this, we would like to introduce two concepts for general CR algorithms, the stable colormap and the partition of a colormap. For any CR algorithm, at each iteration, the color mapping $\chi_{\mathcal{G}}^t$ induces a partition of the vertex set \mathcal{V} with an equivalence relation $\sim_{\chi_{\mathcal{G}}^t}$ defined to be $u \sim_{\chi_{\mathcal{G}}^t} v \Leftrightarrow \chi_{\mathcal{G}}^t(u) = \chi_{\mathcal{G}}^t(v)$ for $u, v \in V$. We call each equivalence class a color class with an associated color $c \in C$, denoted as $(\chi_{\mathcal{G}}^t)^{-1}(c) := \{v \in V : \chi_{\mathcal{G}}^t(v) = c\}$. Formally, we define the partition of any color mapping $\chi_{\mathcal{G}}$

Definition B.4. (Partition) The partition corresponding to $\chi_{\mathcal{G}}$ is the set $P(\chi_{\mathcal{G}}) = \{\chi_{\mathcal{G}}^{-1}(c) : c \in \mathcal{C}_{\mathcal{G}}\}$, where $\mathcal{C}_{\mathcal{G}} := \{\chi_{\mathcal{G}} : v \in V\}$. More specifically, if any element in $P(\chi_{\mathcal{G}}^1)$ is a subset of some element in $P(\chi_{\mathcal{G}}^2)$, we say that $P(\chi_{\mathcal{G}}^1)$ is at least as fine as $P(\chi_{\mathcal{G}}^2)$.

It's easy to see due to the hash function, any color refinement iteration refines the partition $P(\chi_{\mathcal{G}}^t)$ to a finer partition $P(\chi_{\mathcal{G}}^{t+1})$. Since the number of vertices $|V| \leq n$, there must exist an iteration $T < |V|$ such that $P(\chi_{\mathcal{G}}^T) = P(\chi_{\mathcal{G}}^{T+1})$. Formally, we define the stable color mapping and stable partition

Definition B.5. (Stable partition and stable color mapping) Given a graph $\mathcal{G} = (\mathcal{V}, \mathcal{E})$, and an CR refinement $C \in \text{End}(\text{Hom}(\mathcal{V}, \mathcal{C}))$. Starting from $\chi_{\mathcal{G}}^0 = c_0$ (a constant initial color mapping), $\chi_{\mathcal{G}}^{t+1} = C(\chi_{\mathcal{G}}^t)$. There exist an iteration $T < |\mathcal{V}|$, such that $P(\chi_{\mathcal{G}}^T) = P(\chi_{\mathcal{G}}^{T+1})$. Such $P(\chi_{\mathcal{G}}^T)$ is called a stable partition denoted as $P_{\text{stable}}(C)$. Furthermore, we use $\chi_{\mathcal{G}}(C)$ to represent one of the many $\chi_{\mathcal{G}}^{T'}$ with $T' \geq T$, namely the stable color mapping.

CR algorithms decide if the graph pair $(\mathcal{G}, \mathcal{H})$ is isomorphic by comparing the color mapping $\chi_{\mathcal{G}}^T$ and $\chi_{\mathcal{H}}^T$. If the stable partition of CR iteration C^1 is finer than C^2 for any graphs with finite nodes, we can conclude that C^1 is more powerful than C^2 . We refer to [Zhang et al., 2023] for more detail.

Proof. Given **Proposition B.2**, we know that each GPNN layer $l \in [L]$ with $\hat{l} := l \bmod p$ can (under sufficient layers and width conditions) fulfill the coloring process of

$$\mathcal{X}_{\mathcal{G}}^{l+1}(v) = \text{hash}\{(\mathcal{X}_{\mathcal{G}}^l(u), f_{vu}^l) : u \in \mathcal{V}\} \quad (18)$$

We simplify the notation of this color refinement iteration by $C^{\hat{l}} \in \text{End}(\text{Hom}(\mathcal{V}, \mathcal{C}))$

$$\mathcal{X}_{\mathcal{G}}^{l+1} = C^{\hat{l}}(\mathcal{X}_{\mathcal{G}}^l) \quad (19)$$

Now, we define the color refinement iteration for a full recurrent period p for $l = kp, k \in \mathbb{N}$,

$$\mathcal{X}_{\mathcal{G}}^{l+p} = C^p \circ \dots \circ C^1 \circ C^0(\mathcal{X}_{\mathcal{G}}^l) \quad (20)$$

Our goal is to show that the combined color refinement $C_{\text{comb}} = C^p \circ \dots \circ C^1 \circ C^0$ is as powerful as the color refinement in 17 denoted as C_{concat} . In order to achieve that, we will compare the stable partition $P(C_{\text{comb}})$ and $P(C_{\text{concat}})$ on an arbitrary graph $\mathcal{G} = (\mathcal{V}, \mathcal{E})$. For stable coloring $\chi_{\mathcal{G}}(C_{\text{comb}})$ and $\chi_{\mathcal{G}}(C_{\text{concat}})$. For $v_1, v_2 \in \mathcal{V}$, we will prove:

$$\chi_{\mathcal{G}}(C_{\text{comb}})(v_1) = \chi_{\mathcal{G}}(C_{\text{comb}})(v_2) \Leftrightarrow \chi_{\mathcal{G}}(C_{\text{concat}})(v_1) = \chi_{\mathcal{G}}(C_{\text{concat}})(v_2) \quad (21)$$

From the left to right, since the stable partition is unique and denoted as $P_{\mathcal{G}}(\chi_{\mathcal{G}}(C_{\text{comb}}))$. We have:

$$\chi_{\mathcal{G}}(C_{\text{comb}})(v_1) = \chi_{\mathcal{G}}(C_{\text{comb}})(v_2) \Leftrightarrow \exists S \in P_{\mathcal{G}}(\chi_{\mathcal{G}}(C_{\text{comb}})), \text{ s.t. } v_1, v_2 \in S \quad (22)$$

Thus we have $P_{\mathcal{G}}(\chi_{\mathcal{G}}(C_{\text{comb}})) = P_{\mathcal{G}}(C^1 \circ \chi_{\mathcal{G}}(C_{\text{comb}})) = \dots = P_{\mathcal{G}}(C^p \circ \dots \circ C^1 \circ \chi_{\mathcal{G}}(C_{\text{comb}}))$, with $v_1, v_2 \in S$ an element of each of the partitions. Which is equivalent to $C^i(\chi_{\mathcal{G}}(C_{\text{comb}}))(v_1) = C^i(\chi_{\mathcal{G}}(C_{\text{comb}}))(v_2)$, for $i \in [p]$. Write it with hash function notation we have $\text{hash}\{\{\chi_{\mathcal{G}}(C_{\text{comb}})(u), F^i(\mathbf{A}_{\mathcal{G}})_{v_1u}), u \in \mathcal{V}\}\} = \text{hash}\{\{\chi_{\mathcal{G}}(C_{\text{comb}})(u), F^i(\mathbf{A}_{\mathcal{G}})_{v_2u}), u \in \mathcal{V}\}\}$, for $i \in [p]$. Thus we can infer that

$$\begin{aligned} & \text{hash}\{\{\chi_{\mathcal{G}}(C_{\text{comb}})(u), (F^0(\mathbf{A}_{\mathcal{G}})_{v_1u}, F^1(\mathbf{A}_{\mathcal{G}})_{v_1u}, \dots, F^p(\mathbf{A}_{\mathcal{G}})_{v_1u}), u \in \mathcal{V}\}\} \\ &= \text{hash}\{\{\chi_{\mathcal{G}}(C_{\text{comb}})(u), (F^0(\mathbf{A}_{\mathcal{G}})_{v_2u}, F^1(\mathbf{A}_{\mathcal{G}})_{v_2u}, \dots, F^p(\mathbf{A}_{\mathcal{G}})_{v_2u}), u \in \mathcal{V}\}\} \end{aligned}$$

Recall on the right-hand side, that the hash notation of C_{concat} is

$$\begin{aligned} & \text{hash}\{\{\chi_{\mathcal{G}}(C_{\text{concat}})(u), (F^0(\mathbf{A}_{\mathcal{G}})_{v_1u}, F^1(\mathbf{A}_{\mathcal{G}})_{v_1u}, \dots, F^p(\mathbf{A}_{\mathcal{G}})_{v_1u}), u \in \mathcal{V}\}\} \\ &= \text{hash}\{\{\chi_{\mathcal{G}}(C_{\text{concat}})(u), (F^0(\mathbf{A}_{\mathcal{G}})_{v_2u}, F^1(\mathbf{A}_{\mathcal{G}})_{v_2u}, \dots, F^p(\mathbf{A}_{\mathcal{G}})_{v_2u}), u \in \mathcal{V}\}\} \end{aligned}$$

Thus $P(C_{\text{comb}})$ is at least as fine as $P(C_{\text{concat}})$. By which we prove the $\chi_{\mathcal{G}}(C_{\text{comb}})(v_1) = \chi_{\mathcal{G}}(C_{\text{comb}})(v_2) \Rightarrow \chi_{\mathcal{G}}(C_{\text{concat}})(v_1) = \chi_{\mathcal{G}}(C_{\text{concat}})(v_2)$

It is straightforward from left to right since the hash notation of C_{concat} implies each of the C^i iterations holds. We have $\chi_{\mathcal{G}}(C_{\text{comb}})(v_1) = \chi_{\mathcal{G}}(C_{\text{comb}})(v_2) \Leftrightarrow \chi_{\mathcal{G}}(C_{\text{concat}})(v_1) = \chi_{\mathcal{G}}(C_{\text{concat}})(v_2)$. By proving 21, we conclude that C_{comb} is at least as fine as C_{concat} and vice versa, thus C_{comb} is as powerful as C_{concat} .

Substituting $[F(\mathbf{A}_{\mathcal{G}})]_u v$ with fun, we finish our proof. □

C Background

C.1 MPNNs

The message-passing framework [Gilmer et al., 2017a] encapsulates a family of models by defining the message function and update functions. An l -th layer performs the following update:

$$\begin{aligned} m_v^{l+1} &= \sum_{u \in N(v)} M_l(h_v^l, h_u^l, e_{vu}) \\ h_v^{l+1} &= U_l(h_v^l, m_v^{l+1}) \end{aligned} \tag{23}$$

An additional readout function is applied in the final layer, h_v^L . The defining component of the framework is the summation over set $N(v)$, denoting the neighbors of vertex v . The original MPNN [Gilmer et al., 2017b] intended to be broad and thus defines the message function as any function depending on the hidden vertices and edge feature. Despite that broader MPNN family recently extends beyond Eq. 23 [Veličković et al., 2018, Bresson and Laurent, 2018], it can still be handled by adding additional terms or normalization factors. In MPNNs, the message is passed according to the connectivity of the input graph so that the structural information of the graph will be collected.

C.2 Graph Transformers

Instead of being restricted by the input graph, transformers propagate information by attending to the vertex features. Graph transformers extend self-attention formulated as,

$$\text{Attn}(\mathbf{X}) := \text{softmax} \left(\frac{\mathbf{Q}\mathbf{K}^T}{\sqrt{d_{\text{out}}}} \right) \mathbf{V} \in \mathbb{R}^{n \times d_{\text{out}}} \tag{24}$$

Where softmax is applied on each row of the normalized similarity matrix. \mathbf{V} , \mathbf{Q} , and \mathbf{K} represent the value, target, and source vertex features, respectively. One possible limitation in applying self-attention to graphs is the lack of structural information [Dwivedi and Bresson, 2021]. Various approaches have been proposed to address this issue, including combining adjacency matrix with the attention [Ying et al., 2021, Kreuzer et al., 2021b, Rampášek et al., 2022], using graph kernel over neighborhood graph of each node instead of softmax over node features [Chen et al., 2022] or including powerful positional and structural encoding [Ma et al., 2023]. Thus, a defining formalism of graph transformers has yet to be proposed to the best of our knowledge. As a result, GTs, in contrast to MPNNs, have no uniform expressiveness upper-bound defined for the entire family. Expressiveness is usually discussed case by case in terms of models [Zhang et al., 2023, Cai et al., 2023].

C.3 Expressiveness

The expressiveness of Graph Neural Networks (GNNs) indicates the upper bound of their ability to discriminate between different graphs [Xu et al., 2019]. It has been noted that most MPNNs’ expressiveness is bounded by 1-dimensional Weisfeiler Leman (1-WL) graph isomorphism test [Weisfeiler and Leman, 1968, Morris et al., 2019b]. 1-WL is also referred to as the color-refinement algorithm, formulated as

$$\chi_{\mathcal{G}}^t(v) := \text{hash}(\chi_{\mathcal{G}}^{t-1}(v), \{\{\chi_{\mathcal{G}}^{t-1}(u) : u \in \mathcal{N}_{\mathcal{G}}(v)\}\}). \quad (25)$$

The “color map” of graph \mathcal{G} , denoted as $\chi_{\mathcal{G}}$ maps from \mathcal{V} to a set of colors \mathcal{C} . As an iterative algorithm, for each time step t , the color for each vertex is updated by a hash function over a multi-set consisting of all the colors of its neighbors. Even though 1-WL is a powerful test known to distinguish a broad class of graphs, it fails to discriminate some simple graph pairs [Babai and Kucera, 1979]. To obtain expressive GNNs, methods are proposed based on higher-order WL tests [Maron et al., 2019, Morris et al., 2022], subgraph isomorphism/homomorphic counting [Frasca et al., 2022, Bevilacqua et al., 2022, Welke et al., 2023], equivalent polynomial [Puny et al., 2023].

C.4 Ollivier-Ricci Curvature

In differential geometry, Ricci curvature is a fundamental concept related to volume growth and allowing to classify the local characteristic of the space (roughly, whether it is sphere- or hyperboloid-like). Curvature also determines the behavior of parallel lines (whether they converge or diverge), known as geodesic dispersion. Discrete curvatures are analogous constructions for graphs (or more generally, metric spaces) trying to mimic some properties of the continuous curvature.

Ollivier [2009] introduced a notion of curvature for metric spaces that measures the Wasserstein distance between Markov chains, i.e. random walks, defined on two nodes. Let \mathcal{G} be a graph with a distance metric $d_{\mathcal{G}}$, and μ_v be a probability measure on \mathcal{G} for node $v \in \mathcal{V}$. The Ollivier–Ricci curvature of any pair $\{(i, j) | (x, y) \in \mathcal{V}^2, x \neq y\}$ is defined as

$$\kappa_{\text{OR}}(x, y) := 1 - \frac{1}{d_{\mathcal{G}}(x, y)} W_1(\mu_x, \mu_y), \quad (26)$$

where W_1 refers to the first Wasserstein distance between μ_i and μ_j .

Ollivier-ricci curvature is the most prominent discrete curvature on metric spaces which quantifies how the geometry of the manifold deviates from flat (Euclidean) space in terms of the metric structure. Other choices of discrete curvatures include the **Forman–Ricci Curvature**

$$\kappa_{\text{FR}}(x, y) := 4 - d_x - d_y + 3 |\#\Delta|$$

and the **Resistance Curvature**

$$\kappa_{\text{R}}(x, y) := \frac{2(p_x + p_y)}{R_{xy}}.$$

Specifically, we build on our the framework of OR-curvature, due to its intrinsic relation with MPNN and its geometric and spectral properties relating to graph structure.

C.5 Over-squashing and over-smoothing Trade-off

During message-passing, information of distant vertex is cached in vertex features along the path. Some of the vertices end up passing messages growing exponentially with the distance, leading to a potential loss of information known as *over-squashing* [Alon and Yahav, 2020]. [Topping et al., 2022] demonstrates the connection between over-squashing and high negative Ollivier-ricci curvature [Ollivier, 2009] for undirected graphs. On the other hand, stacking multiple message-passing layers can lead to *over-smoothing*, wherein the node embedding from different clusters mixed up, thereby adversely affecting performance [Zhao and Akoglu, 2020, Wenkel et al., 2022].

Trade-off between over-smoothing and over-squashing has been discussed [Giraldo et al., 2022]. The authors show that message-passing converges to a stationary distribution exponentially according to the spectral gap λ_2 . Finally, cheeger inequality provides a well-established connection between λ_2 , and the Cheeger constant – a measure of bottleneck. As a result, reducing over-smoothing may lead to over-squashing, and vice versa.

Graph transformers aggregate information based on attention. Over-squashing is on GTs are less discussed: 1. attention is dynamic across layers and is learned from data 2. analysing tool like Ollivier-ricci curvature could not be applied to asymmetric attention which is adopted by some of recent works.

C.6 Motivation for Unified Framework

The exploration of the intricate relationship between Message Passing (MP) and Attention mechanisms highlights a significant yet underexplored avenue in computational research. A notable absence of detailed inspection within existing works prompts the need for a comprehensive approach. By introducing a unified framework, researchers can embark on a systematic expressiveness assessment routine for models encapsulated within this framework, paving the way for a deeper understanding of their capabilities. This framework not only sheds light on the empirical superiority of Graph Transformers (GTs) over Message Passing Neural Networks (MPNNs) but also serves as a bridge to quantify the improvements each design choice in GTs contributes over MPNNs. Furthermore, this approach offers a higher-level taxonomy of existing methods, fostering an environment conducive to the discovery of superior design choices and models. In essence, this logical progression from identifying a foundational connection

to enhancing model design and expressiveness underlines the transformative potential of a unified analytical framework in advancing the field.

D Related Works

Graph Rewiring has been introduced to combat the over-squashing phenomenon in MPNN. [Topping et al. \[2022\]](#) proposed an iterative graph rewiring algorithm based on Balanced Forman Ricci curvature to mitigate the effect of negatively-curved edges on bottlenecks. [Gutteridge et al. \[2023\]](#) introduced a delayed message passing mechanism, which dynamically performs rewiring on graphs in the form of k -hop skip connections. [Brüel-Gabrielsson et al. \[2022\]](#) employed the strategy to rewire the node to all the other nodes in a receptive field and use positional encoding to describe the original graph structure.

Graph Positional Encodings have been studied to enhance MPNNs [[Zhang et al., 2021](#), [Lim et al., 2023](#), [Wang et al., 2022](#), [Dwivedi et al., 2021](#), [Bouritsas et al., 2022a](#), [Velingker et al., 2022](#), [You et al., 2019](#), [Li et al., 2020](#)], and graph transformers [[Dwivedi and Bresson, 2021](#), [Kreuzer et al., 2021b](#), [Rampásek et al., 2022](#), [Ying et al., 2021](#), [Zhang et al., 2023](#), [Ma et al., 2023](#)] by injecting various graph features, such as spectral information, affinity-measure and geodesic distance.

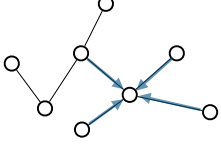
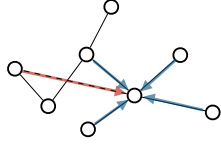
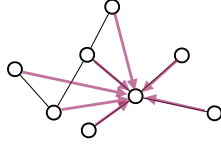
Expressivity is an eternal topic of graph neural networks (GNNs) research. [Xu et al. \[2019\]](#) first points out the expressiveness limitation of MPNNs bounded by 1-WL algorithm on the graph isomorphism test. Follow-up works have attempted to breakthrough via higher-order-GNNs [[Morris et al., 2019a](#), [Maron et al., 2019](#), [Bodnar et al., 2021](#)]. However, those methods usually lead to higher order of complexity. Other approaches include strong structural and positional encoding [[Bouritsas et al., 2022a](#), [Zhang et al., 2023](#)] and subgraph aggregation [[Bevilacqua et al., 2022](#), [Zhou et al., 2023](#)]. Given various methods stating better than 1-WL expressivity, recent methods have started to rethink the WL hierarchy as the default measurement of the expressiveness [[Puny et al., 2023](#), [Zhang et al., 2023](#), [Morris et al., 2022](#)].

Ollivier-Ricci curvature. There are various works investigating the sole mathematical properties of OR-curvatures proposed by [Ollivier \[2009\]](#). [Jost and Liu \[2014\]](#) reveals OR-curvature’s connection with local clustering coefficient on undirected graphs where [Topping et al. \[2022\]](#) utilized to obtain a lower bound estimation for performing graph rewiring. Without restricting it to an unweighted-undirected graph, [Bai et al. \[2020\]](#) extends OR-curvature to weighted graphs by using the weighted graph Laplacian and carries the discussion to continuous-time Ollivier-Ricci flow. [Ozawa et al. \[2020\]](#) extends OR-curvature to strongly-connected weighted-directed graph using Perron measure with canonical shortest distance function, and we extend the curvature to weighted distance function to obtain CURC.

E Generality of GPNN framework

E.1 Taxonomy of Existing Graph Models in GPNNs

Table 4: Demonstration of three different graph model families to showcase the generality of the GPNN framework.

MPNNs	Rewiring	GraphTransformer
		
Taxonomy of Propagation Graphs		
Local Static/Dynamic with/without Feature Feat. Dep./Ind.	Non-Local Static/Dynamic without Feature Feat. Ind.	Global Dynamic with Feature Feat. Dep.

E.2 Existing Models as GPNNs

Notation

- $\mathbf{A} := [a_{ij}]_{i,j \in \mathcal{V}}$ adjacency matrix
- $\mathbf{D} := \text{diag}[d_{ii}]_{i \in \mathcal{V}}$ degree (diagonal) matrix
- $\tilde{\mathbf{A}}, \tilde{\mathbf{D}}$ denote the corresponding matrices with self-loops

We demonstrate how different graph models can be cast into the GPNN framework by defining adjacency functions and connectivity functions. We provide the examples with scalar-valued feature and one propagation graph with further specification, which can be directly extended vector-valued features via multi-head (i.e., multiple propagation matrices) and/or convolution architecture.

We ignore other optional components (e.g., normalization layers, residual connection) in the networks. Without further specification, we assume that $h_i^{l+1} := m_i^{l+1}$, and the superscript of layer index on weight matrices/vectors are dropped for simplicity.

GCN [Kipf and Welling, 2017] generates the propagation matrix by symmetric normalized adjacency matrix with self-loops,

$$\omega_{ij}^{l+1} := \tilde{a}_{ij} \tilde{d}_i^{-1/2} \tilde{d}_j^{-1/2} \quad (27)$$

Propagation Graph	Static	Dynamic
Local	GCN [Kipf and Welling, 2017], GraphSAGE [Hamilton et al., 2017], GIN [Xu et al., 2019]	MoNet [Monti et al., 2017], GAT* [Veličković et al., 2018], GatedGCN* [Bresson and Laurent, 2018]
Non-Local	SDRF [Topping et al., 2022] GDC [Gasteiger et al., 2019]	Drew [Gutteridge et al., 2023] LASER [Barbero et al., 2023] ChebNet [Defferrard et al., 2016], BernNet [Barbero et al., 2022], JacobConv [Wang and Zhang, 2022] SIGN [Frasca et al., 2020], ADC [Zhao et al., 2022] Exphormer* [Shirzad et al., 2023b], MPNN+VN* [Cai et al., 2023], GPS-BigBird* [Rampásek et al., 2022]
Global	DeepSet [Zaheer et al., 2017]	Spectral GCN [Bruna et al., 2014], Specformer [Bo et al., 2023], SANs* [Kreuzer et al., 2021b], Graphormer* [Ying et al., 2021], GraphGPS-Full* [Rampásek et al., 2022], EGT* [Hussain et al., 2022], GRIT* [Ma et al., 2023]

Table 5: Taxonomy in GPNN Framework

*: denotes that the propagation matrices are conditional on the node feature. We disregard the impact of residual connections in
MPNNs, Graph Rewiring, Diffusion Enhanced GNNs, Polynomial Spectral GNN,
Full Spectral GNNs, Graph Transformers, Approximated/Efficient Graph Transformers

MoNet [Monti et al., 2017] proposes to generate the propagation matrix as a Gaussian kernel based on “pseudo-coordinate” between two adjacent nodes, which is $[d_i^{-1}, d_j^{-1}]$, $\forall (v, u) \in \mathcal{E}$,

$$\omega_{ij}^{l+1} = \tilde{a}_{ij} \cdot \exp\left(-\frac{1}{2}(\tilde{\mathbf{u}}_{ij} - \boldsymbol{\mu})^\top \boldsymbol{\Sigma}^{-1}(\tilde{\mathbf{u}}_{ij} - \boldsymbol{\mu})\right) \quad (28)$$

where $\tilde{\mathbf{u}}_{ij} = \mathbf{W} \cdot [d_i^{-1}, d_j^{-1}]^\top + \mathbf{b}$

and $\mathbf{W} \in \mathbb{R}^{r \times 2}$, $\mathbf{b} \in \mathbb{R}^r$, $\boldsymbol{\mu} \in \mathbb{R}^r$ and $\boldsymbol{\Sigma} \in \mathbb{R}^{r \times r}$ are learnable parameters.

GraphSAGE-GCN [Hamilton et al., 2017] generates the propagation matrix via row-normalized adjacency matrix with self-loops,

$$\omega_{ij}^{l+1} = \tilde{a}_{ij} \tilde{d}_i^{-1}. \quad (29)$$

GraphSAGE-Average [Hamilton et al., 2017] generates the propagation matrix, similar to GraphSAGE-GCN, by the row-normalized adjacency matrix

without self-loops and self-loops with extra learnable parameters,

$$\begin{aligned}\omega_{ij}^{l+1} &= a_{ij}d_i^{-1} \\ h_i^{l+1} &= \mathbf{W}_1 h_i^l + \mathbf{W}_2 m_j^{l+1}\end{aligned}\quad (30)$$

where $\mathbf{W}_1, \mathbf{W}_2 \in \mathbb{R}^{c \times c}$ are learnable matrices.

GIN [Xu et al., 2019] generates the propagation matrix based on the unnormalized adjacency matrix and an extra learnable parameter for self-loops,

$$\begin{aligned}\omega_{ij}^{l+1} &= a_{ij} \\ h_v^{l+1} &= (1 - \theta_0)h_v^l + \theta_1 m_v^{l+1}\end{aligned}\quad (31)$$

where $\theta_0, \theta_1 \in \mathbb{R}$ are learnable parameters.

GAT [Veličković et al., 2018] generate the propagation matrix based on the attention mechanism on the observed edges,

$$\omega_{ij}^{l+1} = \tilde{a}_{ij} \text{Softmax}_{j' \in \{j' | \tilde{a}_{ij'} = 1\}} (\text{LeakyReLU}(\mathbf{w}_1^\top \mathbf{W} \mathbf{x}_i + \mathbf{w}_2^\top \mathbf{W} \mathbf{x}_j)) \quad (32)$$

where node representation $\mathbf{x}_i \in \mathbb{R}^d$,

GatedGCN [Bresson and Laurent, 2018, Dwivedi et al., 2022a], similar to GAT, include semantic information into the propagation matrix via the (normalized) gating mechanism,

$$\begin{aligned}\omega_{ij}^{l+1} &= \tilde{a}_{ij} \cdot \frac{u_{ij}}{\sum_{j' \in \{j' | \tilde{a}_{ij'} = 1\}} u_{ij'}} \\ \text{where } u_{ij} &= \sigma(\mathbf{w}_1^\top \mathbf{x}_i + \mathbf{w}_2^\top \mathbf{x}_j) \\ h_i^{l+1} &= \theta_1 h_i^l + \theta_2 m_j^{l+1}\end{aligned}\quad (33)$$

where σ denotes the Sigmoid operation; $\theta_0, \theta_1 \in \mathbb{R}$ are learnable scalar; $\mathbf{w}_1, \mathbf{w}_2 \in \mathbb{R}^r$ are weight vectors; $\mathbf{x}_i \in \mathbb{R}^d$ stands for the node representation.

(Graph Rewiring) Drew [Gutteridge et al., 2023] proposes to generate the propagation matrix by rewiring to nodes in top- L -hop neighborhood for L -th layer,

$$\begin{aligned}\omega_{ij}^{l+1} &= \begin{cases} \frac{\theta_k}{|\{j' | d_{\mathcal{G}}(i, j') = k\}|} & \text{if } d_{\mathcal{G}}(i, j) = k. \\ 0 & \text{otherwise} \end{cases} \\ k &= 1, \dots, L, \\ h_i^{l+1} &= \theta_0 h_i^l + m_j^j\end{aligned}\quad (34)$$

where $d_{\mathcal{G}} : \mathcal{V} \times \mathcal{V} \rightarrow \mathbf{Z}_{\geq 0}$ denotes the shortest-path distance on graphs; $\theta_1, \dots, \theta_L \in \mathbb{R}$ are learnable weights.

(Polynomial Spectral GNN) ChebNet [Defferrard et al., 2016] generate the propagation matrix as the approximation to Laplacian eigenvectors via the Chebyshev polynomial, which can be viewed as the top- K power of the normalized $\mathbf{L} = \mathbf{D} - \mathbf{A}$,

$$\omega_{ij}^{l+1} = \sum_{k=0}^{K-1} \theta_k \tau_{ij}^k \quad (35)$$

where τ_{ij}^k is the i, j -element of the $T_k(\tilde{L})$, in which, $\tilde{L} := (\mathbf{D} - \mathbf{A}) / \lambda_{\max} - \mathbf{I}$ is the normalized Laplacian matrix by the largest eigenvalue and $T_k(x) := 2xT_{k-1}(x) - T_{k-2}(x)$ is the Chebyshev polynomial of order k .

SANs [Kreuzer et al., 2021a]

$$\omega_{ij}^{l+1} = \text{Softmax}_{j \in \mathcal{V}} ((\mathbf{W}_1(\mathbf{x}_i + \mathbf{e}_i))^{\top} (\mathbf{W}_2(\mathbf{x}_j + \mathbf{e}_j))) \quad (36)$$

where $\mathbf{W}_1, \mathbf{W}_2 \in \mathbb{R}^{r \times d}$ are learnable weight matrices; $\mathbf{e}_i \in \mathbb{R}^d$ stands for the positional encoding for node i . Note that, the scaling factor in scaled dot-product is ignored for simplicity, same for the following.

Graphormer [Ying et al., 2021]

$$\omega_{ij}^{l+1} = \text{Softmax}_{j \in \mathcal{V}} ((\mathbf{W}_1 \mathbf{x}_i)^{\top} (\mathbf{W}_2 \mathbf{x}_j) + \mathbf{w}^{\top} \mathbf{e}_{ij}) \quad (37)$$

where $\mathbf{W}_1, \mathbf{W}_2 \in \mathbb{R}^{r \times d}$ and $\mathbf{w} \in \mathbb{R}^d$ are learnable weight matrices/vectors; $\mathbf{e}_{ij} \in \mathbb{R}^d$ stands for the positional encoding and/or edge-attributes between node i and node j .

GRIT [Ma et al., 2023]

$$\omega_{ij}^{l+1} = \mathbf{w}^{\top} \text{ReLU}(\rho((\mathbf{W}_1 \mathbf{x}_i + \mathbf{W}_2 \mathbf{x}_j) \odot \mathbf{W}_3 \mathbf{e}_{ij}) + \mathbf{W}_4 \mathbf{e}_{ij}) \quad (38)$$

where $\mathbf{W}_1, \mathbf{W}_2, \mathbf{W}_3, \mathbf{W}_4 \in \mathbb{R}^{r \times d}$ and $\mathbf{w} \in \mathbb{R}^r$ are learnable weight matrices/vectors; $\mathbf{e}_{ij} \in \mathbb{R}^d$ stands for the positional encoding and/or edge-attributes between node i and node j .

F Experimental Details

F.1 Details of GPNN-PE

F.1.1 Model Architecture

To verify our theoretical findings, we build up a purely structural-based GPNN, called GPNN-PE, based on the SOTA GTs - GRIT [Ma et al., 2023], by removing the *query-key architecture* which models the token similarity on node representations.

In each layer, we update node representations $\mathbf{x}_u \forall u \in \mathcal{V}$ and node-pair representations $\mathbf{e}_{u,v}, \forall u, v \in \mathcal{V}$. Similar to GRIT, we initialize these using the initial node features and our RRWP positional encodings: $\mathbf{x}_i = [\mathbf{x}'_i \parallel \mathbf{P}_{i,i}] \in \mathbb{R}^{d_h+K}$ and $\mathbf{e}_{i,j} = [\mathbf{e}'_{i,j} \parallel \mathbf{P}_{i,j}] \in \mathbb{R}^{d_e+K}$, where $\mathbf{x}'_i \in \mathbb{R}^{d_h}$ and $\mathbf{e}'_{i,j} \in \mathbb{R}^{d_e}$ are observed node and edge attributes, respectively; $\mathbf{P}_{i,j}$ is the relative positional encoding for graphs. Note that, if node/edge attributes are not present in the data, we can set $\mathbf{x}'_i/\mathbf{e}'_{i,j}$ as zero-vectors $\mathbf{0} \in \mathbb{R}^d$. We set $\mathbf{e}'_{i,j} = \mathbf{0}$ if there is no observed edge from i to j in the original graph.

We replace the original attention computation in GRIT with a multi-layer perceptron (MLP):

$$\begin{aligned} \hat{\mathbf{e}}_{i,j} &= \sigma(\mathbf{W}_1 \mathbf{e}_{i,j}) \in \mathbb{R}^{d'}, \\ \alpha_{ij} &= \text{Softmax}_{j \in \mathcal{V}}(\mathbf{W}_2 \hat{\mathbf{e}}_{i,j}) \in \mathbb{R}, \\ \hat{\mathbf{x}}_i &= \sum_{j \in \mathcal{V}} \alpha_{ij} \cdot (\mathbf{W}_3 \mathbf{x}_j + \mathbf{W}_4 \hat{\mathbf{e}}_{i,j}) \in \mathbb{R}^{d'}, \end{aligned} \tag{39}$$

where σ is a non-linear activation (ReLU by default); $\mathbf{W}_1 \in \mathbb{R}^{d' \times d}$, $\mathbf{W}_2 \in \mathbb{R}^{1 \times d'}$, $\mathbf{W}_3 \in \mathbb{R}^{d'' \times d}$ and $\mathbf{W}_4 \in \mathbb{R}^{d'' \times d'}$ are learnable weight matrices.

Following GRIT, we retain the update of edges and the multiple heads (say, N_h heads) without further specification:

$$\begin{aligned} \mathbf{x}_i^{\text{out}} &= \sum_{h=1}^{N_h} \mathbf{W}_O^h \hat{\mathbf{x}}_i^h \in \mathbb{R}^d, \\ \mathbf{e}_{i,j}^{\text{out}} &= \sum_{h=1}^{N_h} \mathbf{W}_{Eo}^h \hat{\mathbf{e}}_{i,j}^h \in \mathbb{R}^d, \end{aligned} \tag{40}$$

where $\mathbf{W}_O^h, \mathbf{W}_{Eo}^h \in \mathbb{R}^{d \times d''}$ are output weight matrices for each head h .

F.1.2 Positional Encoding

In this work, we apply Relative Random walk positional encoding utilized in GRIT [Ma et al., 2023], which is one of the most expressive graph positional encoding. Let $\mathbf{A} \in \mathbb{R}^{n \times n}$ be the adjacency matrix of a graph $(\mathcal{V}, \mathcal{E})$ with n nodes, and let \mathbf{D} be the diagonal degree matrix. Define $\mathbf{M} := \mathbf{D}^{-1} \mathbf{A}$, and note that \mathbf{M}_{ij} is the probability that i hops to j in one step of a simple random walk. The

proposed relative random walk probabilities (RRWP) initial positional encoding is defined for each pair of nodes $i, j \in \mathcal{V}$ as follows:

$$\mathbf{P}_{i,j} = [\mathbf{I}, \mathbf{M}, \mathbf{M}^2, \dots, \mathbf{M}^{k-1}]_{i,j} \in \mathbb{R}^k, \quad (41)$$

in which \mathbf{I} is the identity matrix. In other words, in GPNN-PE, $\psi : \mathbb{R}^{n \times n} \rightarrow \mathbb{R}^{n \times n \times k}$ is defined as

$$\psi(\mathbf{A})_{i,j} := [\mathbf{I}, \mathbf{D}^{-1}\mathbf{A}, (\mathbf{D}^{-1}\mathbf{A})^2, \dots, (\mathbf{D}^{-1}\mathbf{A})^{k-1}]_{i,j} \quad (42)$$

F.2 More about Experimental

F.2.1 Baselines

We primarily compare our methods with the SOTA graph transformer, GRIT [Ma et al., 2023], as well as a number of prevalent graph-learning models: popular message-passing neural networks (GCN [Kipf and Welling, 2017], GIN [Xu et al., 2019] and its variant with edge-features [Hu et al., 2020], GAT [Veličković et al., 2018], GatedGCN [Bresson and Laurent, 2018], GatedGCN-LSPE [Dwivedi et al., 2021], PNA [Corso et al., 2020]); Graph Transformers (Graphormer [Ying et al., 2021], K-Subgraph SAT [Chen et al., 2022], EGT [Hussain et al., 2022], SAN [Kreuzer et al., 2021a], Graphormer-URPE [Luo et al., 2022], Graphormer-GD [Zhang et al., 2023], GraphGPS [Rampásek et al., 2022]); and other recent Graph Neural Networks with SOTA performance (DGN [Beani et al., 2021], GSN [Bouritsas et al., 2022b], CIN [Bodnar et al., 2021], CRaW1 [Toenshoff et al., 2021], GIN-AK+ [Zhao et al., 2021b]).

F.2.2 Extended Experimental Results

We also evaluate GPNN-PE on on five datasets from the Benchmarking GNNs work [Dwivedi et al., 2022a] (as shown in Table 6). These datasets are among the most widely used graph benchmarks and cover diverse graph learning tasks, including node classification, graph classification, and graph regression, with a focus on graph structure and long-range dependencies.

F.2.3 Descriptions of Datasets

A summary of the statistics and characteristics of datasets is shown in Table 7. The first five datasets are from Dwivedi et al. [2022a] and the last two are from Dwivedi et al. [2022b]. Readers are referred to Dwivedi et al. [2022a] and Dwivedi et al. [2022b] for more details about the datasets.

F.2.4 Dataset splits and random seed

Our experiments are conducted on the standard train/validation/test splits of the evaluated benchmarks. For each dataset, we execute 4 runs with different random seeds (0,1,2,3) and report the mean performance and standard deviation.

Table 6: Test performance in five benchmarks from [Dwivedi et al., 2022a]. Shown is the mean \pm s.d. of 4 runs with different random seeds. Highlighted are the top **first**, **second**, and **third** results. # Param $\sim 500K$ for ZINC, PATTERN, CLUSTER and $\sim 100K$ for MNIST and CIFAR10.

Model	ZINC	MNIST	CIFAR10	PATTERN	CLUSTER
	MAE \downarrow	Accuracy \uparrow	Accuracy \uparrow	Accuracy \uparrow	Accuracy \uparrow
GCN	0.367 \pm 0.011	90.705 \pm 0.218	55.710 \pm 0.381	71.892 \pm 0.334	68.498 \pm 0.976
GIN	0.526 \pm 0.051	96.485 \pm 0.252	55.255 \pm 1.527	85.387 \pm 0.136	64.716 \pm 1.553
GAT	0.384 \pm 0.007	95.535 \pm 0.205	64.223 \pm 0.455	78.271 \pm 0.186	70.587 \pm 0.447
GatedGCN	0.282 \pm 0.015	97.340 \pm 0.143	67.312 \pm 0.311	85.568 \pm 0.088	73.840 \pm 0.326
GatedGCN-LSPE	0.090 \pm 0.001	–	–	–	–
SAN	0.139 \pm 0.006	–	–	86.581 \pm 0.037	76.691 \pm 0.65
Graphormer	0.122 \pm 0.006	–	–	–	–
Graphormer-GD	0.081 \pm 0.009	–	–	–	–
GPS	0.070 \pm 0.004	98.051 \pm 0.126	72.298 \pm 0.356	86.685 \pm 0.059	78.016 \pm 0.180
GRIT	0.059 \pm 0.002	98.108 \pm 0.111	76.468 \pm 0.881	87.196 \pm 0.076	80.026 \pm 0.277
GPNN-PE	0.060 \pm 0.003	98.165 \pm 0.077	75.505 \pm 0.642	87.083 \pm 0.035	78.878 \pm 0.152
+ static	0.064 \pm 0.002	98.018 \pm 0.024	75.050, 0.282	87.045 \pm 0.032	78.830 \pm 0.127
+ 1-head	0.066 \pm 0.005	97.560 \pm 0.090	72.042 \pm 0.714	86.965 \pm 0.043	78.373 \pm 0.212

Table 7: Overview of the graph learning datasets involved in this work [Dwivedi et al., 2022a,b, Irwin et al., 2012, Hu et al., 2021] .

Dataset	# Graphs	Avg. # nodes	Avg. # edges	Directed	Prediction level	Prediction task	Metric
ZINC	12,000	23.2	24.9	No	graph	regression	Mean Abs. Error
MNIST	70,000	70.6	564.5	Yes	graph	10-class classif.	Accuracy
CIFAR10	60,000	117.6	941.1	Yes	graph	10-class classif.	Accuracy
PATTERN	14,000	118.9	3,039.3	No	inductive node	binary classif.	Weighted Accuracy
CLUSTER	12,000	117.2	2,150.9	No	inductive node	6-class classif.	Accuracy
Peptides-func	15,535	150.9	307.3	No	graph	10-task classif.	Avg. Precision
Peptides-struct	15,535	150.9	307.3	No	graph	11-task regression	Mean Abs. Error

F.2.5 Hyperparameters

Due to the limited time and computational resources, we did not perform an exhaustive search or a grid search on the hyperparameters. We mainly follow the hyperparameter setting of GRIT [Ma et al., 2023] and make slight changes to fit the number of parameters into the commonly used parameter budgets. For the benchmarks from [Dwivedi et al., 2022a,b], we follow the most commonly used parameter budgets: up to 500k parameters for ZINC, PATTERN, CLUSTER, Peptides-func and Peptides-struct; and $\sim 100k$ parameters for MNIST and CIFAR10.

The final hyperparameters are presented in Tables. 8 and Tables. 9.

F.3 Visualization of Curvature

We visualize the trend curves of minimum/average CURC given the attention matrices across the first 32 test graphs in ZINC, as shown in Fig. 5 and Fig. 6.

Table 8: Hyperparameters for five datasets from BenchmarkingGNNs [Dwivedi et al., 2022a].

Hyperparameter	ZINC	MNIST	CIFAR10	PATTERN	CLUSTER
# Transformer Layers	10	4	4	10	16
Hidden dim	64	52	52	64	48
# Heads	8	4	4	8	8
Dropout	0	0	0	0	0.01
Attention dropout	0.2	0.5	0.5	0.2	0.5
Graph pooling	sum	mean	mean	–	–
PE dim (RW-steps)	21	18	18	21	32
PE encoder	linear	linear	linear	linear	linear
Batch size	32/256	16	16	32	16
Learning Rate	0.001	0.001	0.001	0.0005	0.0005
# Epochs	2000	200	200	100	100
# Warmup epochs	50	5	5	5	5
Weight decay	1e – 5	1e – 5	1e – 5	1e – 5	1e – 5
# Parameters	417,877	100,754,	98,238	353, 877	319,670
# Param. (1 Head)	385,237	108,866	106,350	389,717	351,926
# Param. (Share Attn)	311,381	92,330	89,814	315,861	283,670

Table 9: Hyperparameters for two datasets from the Long-range Graph Benchmark [Dwivedi et al., 2022b]

Hyperparameter	Peptides-func	Peptides-struct
# Transformer Layers	4	4
Hidden dim	96	96
# Heads	4	8
Dropout	0	0
Attention dropout	0.2	0.2
Graph pooling	mean	mean
PE dim (walk-step)	17	24
PE encoder	linear	linear
Batch size	32	32
Learning Rate	0.0003	0.0003
# Epochs	200	200
# Warmup epochs	5	5
Weight decay	0	0
# Parameters	332,142	338,315
# Param. (1 Head)	370,571	360,574
# Param. (Share Attn)	310,091	304,702

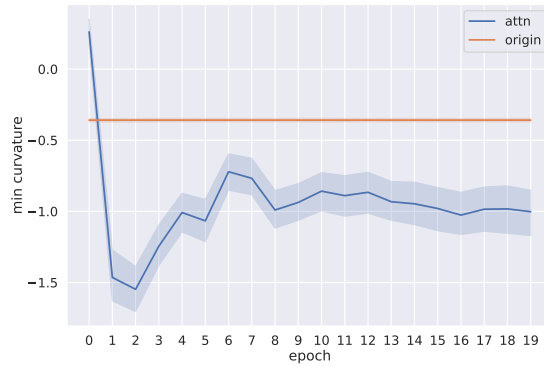


Figure 5: The trend of Minimum CURC for the first 32 test graphs in ZINC. Shade is the Confidence Interval at the 95% confidence level.

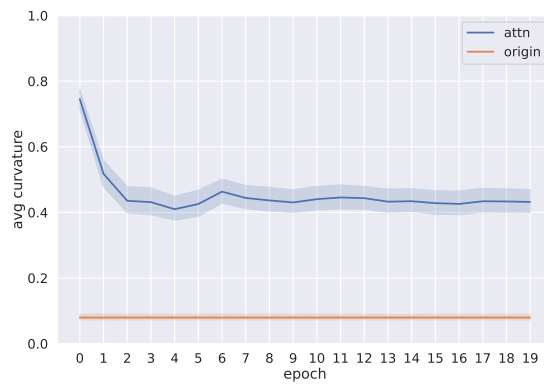


Figure 6: The trend of Average CURC for the first 32 test graphs in ZINC. Shade is the Confidence Interval at the 95% confidence level.